Reconstruction models of cubic SiC surfaces

2004 J. Phys.: Condens. Matter 16 S1659

(http://iopscience.iop.org/0953-8984/16/17/012)

INSTITUTE OF PHYSICS PUBLISHING JOURNAL OF PHYSICS: CONDENSED MATTER

J. Phys.: Condens. Matter **16** (2004) S1659–S1703 PII: S0953-8984(04)65100-9

Reconstruction models of cubic SiC surfaces

Johannes Pollmann and Peter Krüger

Institut für Festkörpertheorie, Universität Münster, D-48149 Münster, Germany

E-mail: pollman@uni-muenster.de

Received 24 June 2003
Published 16 April 2004
Online at stacks.iop.org/JPhysCM/16/S1659
DOI: 10.1088/0953-8984/16/17/012

Abstract

The current understanding of the relaxation and reconstruction of low-index cubic SiC surfaces, as it derives from first-principles calculations, is briefly reviewed in comparison with surface-sensitive experimental data. The calculated structural properties are obtained from *ab initio* total energy and grand canonical potential minimization in the framework of the local density and generalized gradient approximations of density functional theory. Characteristic surface structural properties are related to the surface electronic structure and to the ionicity of the underlying bulk crystal. For a number of cubic surfaces, there is good agreement between first-principles results and the data. In other cases, most noticeably for Si-terminated SiC(001) surfaces, there is still considerable controversy with respect to the atomic and electronic structure in both experiment and theory.

(Some figures in this article are in colour only in the electronic version)

Contents

1. Introduction

Silicon carbide is a technologically important and fundamentally interesting group IV compound semiconductor. It is fairly ionic, residing at the borderline between covalent elemental and ionic compound semiconductors. While the former crystallize in either the diamond or zincblende structure the latter occur in the wurtzite or sodium chloride structure. SiC—lying in between—occurs in an extremely large number of polytypes (see [1]), the cubic and the hexagonal of which are the most important for technological applications. Their basic properties and the wide spectrum of their applications in micro- and optoelectronics have been described at length, for example, in a collection of review articles [2]. The very basis for such applications is the specific electronic structure of the SiC polytypes and their surfaces [3, 4]. Thus, a thorough knowledge of the physical properties of SiC polytypes and their surfaces is a matter of both fundamental interest and technological importance. Detailed accounts of the experimental and theoretical literature addressing fundamental properties of SiC polytypes and their surfaces may be found in a host of review articles [1–10]. In spite of the considerable amount of work on SiC surfaces, a number of basic questions related to their atomic and electronic structure are not conclusively resolved to date. The results of advanced experimental and theoretical techniques are still controversial, in cases calling for improved surface structural models and making the field truly fascinating from a basic scientific point of view. For some of the technologically most important SiC surfaces—like Si-terminated SiC(001)-c(4×2)—there is not even full agreement on the gross features of their reconstruction. This topic has been dealt with, as well, in a very recent review by Catellani and Galli employing the results of first-principles molecular dynamics (FP-MD) simulations [9]. In this paper, we concentrate on a discussion of more recent first-principles calculations with particular emphasis on structural and electronic properties of cubic SiC surfaces. Theoretical *ab initio* results and surface microscopy and spectroscopy data are addressed in direct comparison aiming at an assessment of solved and open questions, respectively.

Cubic SiC, often labelled as β-SiC or 3C-SiC, crystallizes in the zincblende structure with a bulk lattice constant of 4.36 Å, which is about 20% smaller than that of Si (5.43 Å) and roughly 22% larger than that of diamond (3.57 Å). The Si–C bond length is 1.89 Å. The different strengths of the C and Si potentials give rise to a charge transfer from the Si to the C atoms. As a consequence, the electronic charge density distribution along the Si–C bonds is strongly asymmetric, leading to a considerable ionicity [11]. Therefore, Si atoms behave like cations while C atoms behave like anions in SiC. The bulk-bond length of 1.89 Å is about 3% smaller than the sum of the covalent radii of Si (1.17 Å) and C (0.77 Å) atoms, amounting to 1.94 Å. The charge transfer obviously reduces the effective covalent radius of the Si cations more strongly than it increases the effective covalent radius of the C anions. The ionicity of SiC gives rise to an ionic gap within the valence bands of its bulk band structure [1, 5] contrary to elemental semiconductors but very similar to heteropolar III–V or more ionic II–VI compound semiconductors.

The pronounced ionicity of SiC is of particular importance for the relaxation and reconstruction of SiC surfaces. As a consequence of the ionicity, there are polar and nonpolar cubic SiC surfaces. At the polar (111) and (001) surfaces, Si and C layers alternate along the [111]- and [001] directions, respectively. Thus, there are two distinctly different cubic SiC surfaces in each case which are commonly referred to as Si- or C-terminated surfaces, or for brevity as Si face and C face, respectively. At the Si face or the C face one encounters Si or C orbitals on a two-dimensional lattice whose lattice constant is much smaller or much larger than that of the related elemental Si or diamond surfaces, respectively. Therefore, characteristically different reconstructions occur at cubic SiC surfaces, as compared to those

of the respective Si and diamond surfaces. In addition, Si- and C-terminated cubic SiC surfaces show largely different reconstructions with respect to one another. This is related to the fact that the structural changes of the bulk tetrahedral configuration, i.e. the bond-length and bond-angle changes occurring upon reconstruction, involve much larger energy around C than around Si atoms due to the much stronger localization of the C valence states, as opposed to the Si valence states.

Depending on the surface orientation, the stoichiometry and the actual growth and surface preparation conditions 1×1, 2×1, c(2×2), c(4×2), 3×2, $(\sqrt{3} \times \sqrt{3})$R30°, 3×3, 5×2, 7×2, 8×2 and 15×2 structures have been observed. Among these, both C- and Si-rich structures have been identified and investigated in experiment by a whole variety of surface microscopy and spectroscopy methods. The status of experimental research on cubic SiC surfaces up to 1996 has been reviewed by Bermudez [4] and very recently, with particular emphasis on scanning tunnelling microscopy (STM) and photoelectron spectroscopy (PES) results for SiC(001) surfaces, by Soukiassian [10].

In the present paper, we first very briefly summarize the theoretical framework of current *ab initio* atomic and electronic structure calculations of cubic SiC surfaces. Next we address the relaxation of the nonpolar SiC(110) surface. In section 4 we briefly describe current models of the relaxation and reconstruction of SiC(111). In section 5 we present and discuss a number of reconstruction models of C- and Si-terminated SiC(001) surfaces in some detail and address the respective electronic structures in the light of available experimental data. The paper closes with brief conclusions.

2. Calculational methods

Most of the more recent first-principles calculations of structural and electronic properties of SiC surfaces have been carried out employing the local density approximation (LDA) or the generalized gradient approximation (GGA) of density functional theory (DFT). A few quasiparticle band structure calculations within the GW approximation of many-body perturbation theory have been reported, as well [12, 13]. Within DFT-LDA [14, 15], the exchange–correlation potential of Ceperley–Alder [16], as parametrized by Perdew and Zunger [17], is used. In DFT-GGA calculations, exchange–correlation functionals, e.g. as proposed by Perdew *et al* [18], are employed. The external potential of the Si and C ions is usually described by smooth nonlocal pseudopotentials [19–21] in separable form, as suggested by Kleinman and Bylander [22]. As basis sets for expanding the wavefunctions, plane waves (see [9, 23–28]) or linear combinations of Gaussian orbitals (see [8, 11, 12, 29]) are used. Most authors employ the supercell method for calculating optimal surface structures. Supercells containing up to 30 atomic layers and 10 Å of vacuum region have been considered.

Optimal atomic configurations of stoichiometric surfaces are routinely calculated by minimizing the total energy E with respect to all structural degrees of freedom. This is achieved by eliminating the forces on all atoms in the system corresponding to a minimum of E in configuration space [30–32]. The total energy is usually calculated self-consistently within the momentum-space formalism of Ihm *et al* [30]. Actually, a certain number of SiC layers are kept fixed in their bulk configuration in the centre of the supercell and the surface structure is optimized iteratively [33] by moving the atoms on sufficiently many layers at and near the surface until all forces on the respective atoms vanish within a chosen accuracy. When a Gaussian basis set is employed, Pulay forces have to be taken into account in addition to the Hellmann–Feynman forces [31, 32]. A very powerful alternative for surface structure optimizations are FP-MD simulations [34, 35]. It has turned out in the calculations that employing a sufficiently large number of $\boldsymbol{k}_{\parallel}$ points in the surface Brillouin zone (SBZ) is crucial

for convergent surface-structure determinations. This can be achieved either by considering a sufficiently large number of $\boldsymbol{k}_{\parallel}$ points in the original SBZ or by using Γ-point sampling for an artificially enlarged surface unit cell, yielding a correspondingly reduced SBZ. The latter technique has been used mostly in the FP-MD calculations [9]. Using Γ-point sampling in the original SBZ, only, is often not sufficient.

To optimize the structure of nonstoichiometric surfaces, the grand canonical potential Ω has to be minimized instead of the total energy E since the number and species of adatoms (Si or C) are different for different adsorption geometries to be compared [36, 37]. The grand canonical potential Ω for a nonstoichiometric surface is given by

$$\Omega = E - \mu_C n_C - \mu_{Si} n_{Si}$$

where μ_C and μ_{Si} are the chemical potentials of the C and Si atoms in the gas phase and n_C and n_{Si} are the numbers of C and Si atoms in the supercell. The surface preparation conditions determine the actual values of μ_C and μ_{Si}. In thermal equilibrium the SiC substrate acts as a particle reservoir and can exchange Si and C atoms with the gas phase. As a consequence, the chemical potentials of the constituents of the system fulfil the law of mass action $\mu_{Si} + \mu_C = \mu_{SiC(bulk)}$. In addition, the chemical potentials of the respective bulk crystals are related by $\mu_{SiC(bulk)} = \mu_{Si(bulk)} + \mu_{C(bulk)} - \Delta H^f_{SiC}$, where ΔH^f_{SiC} is the formation enthalpy or heat of formation of the SiC bulk crystal. The experimental value of ΔH^f_{SiC} for cubic bulk SiC is 0.72 eV [38]. The above relations allow us to eliminate either μ_C or μ_{Si} from the grand canonical potential Ω which is then determined, for example, by the chemical potential μ_{Si} of the Si atoms in the gas phase, alone. The thermodynamically allowed region of μ_{Si} is restricted to the range

$$\mu_{Si(bulk)} - \Delta H^f_{SiC} \leqslant \mu_{Si} \leqslant \mu_{Si(bulk)}.$$

The experimental value of ΔH^f_{SiC} defines the physically allowed range of possible variations of μ_{Si}. Si-rich (C-poor) preparation conditions correspond to the upper limit $\mu_{Si} = \mu_{Si(bulk)}$ while Si-poor (C-rich) conditions correspond to the lower limit $\mu_{Si} = \mu_{Si(bulk)} - \Delta H^f_{SiC}$. This scheme has been used widely to determine optimal configurations of nonstoichiometric SiC surfaces (see [8, 9, 27, 29]).

For an optimized surface atomic structure the respective surface electronic structure is usually evaluated employing the same supercells as before. However, if the electronic spectrum mainly consists of surface resonances whose wavefunctions can be very extended perpendicular to the surface it is advantageous to refer to potential scattering theory [39, 40]. This approach solves the Kohn–Sham equations for a semi-infinite system self-consistently by treating the reconstructed surface as a two-dimensionally periodic perturbation of a bulk crystal. The secular equation corresponding to the wavefunction expansion into Gaussian orbitals is solved by calculation of its inverse or Green function. The Green function contains full information on the one-particle spectrum of the surface system and allows the calculation of the surface band structure with an extreme spectral resolution [32, 40].

STM images are nowadays routinely calculated in the framework of the Tersoff–Hamann approach [41]. In this approach constant current mode STM images are simulated by calculating topograms of constant charge density above the surface.

3. Nonpolar SiC(110) surface

The cubic modification of SiC exhibits one nonpolar low-index surface, SiC(110), which is, in general, largely similar to the related (110) surfaces of III–V compound semiconductors, like GaAs(110) [11]. The nonpolar SiC(110) surface shows only a relaxation rather than

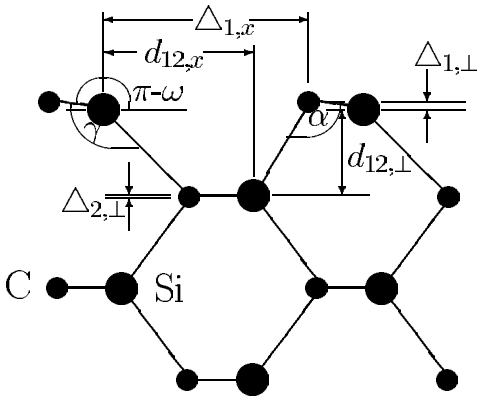

Figure 1. Side view of the relaxed SiC(110)-(1 × 1) surface (from [7, 11]).

a reconstruction. The optimal surface structure of SiC(110) is schematically shown by a side view in figure 1. The most important structural parameter characterizing this relaxation is the top-layer bond-rotation angle ω. It is given by the angle between the projection of the SiC surface bond onto the drawing plane in figure 1 and the surface plane. In general (see [8, 11]), for heteropolar covalent systems, like III–V semiconductor surfaces, quantum mechanical hybridization effects dominate the relaxation, giving rise to relatively large bond-rotation angles ω and the anion–cation bond length is nearly preserved at the surface. If the system becomes more ionic, like SiC(110), the classical Coulomb attraction between anions and cations starts to dominate the relaxation process and the system tends to form more planar cation-anion arrays at the surface with correspondingly smaller ω values. The anion–cation bond length in the surface layer contracts accordingly and a bond-length-contracting rotation relaxation results. The rotation of the surface-layer bonds leads to a raising of the energetic position of empty cation-derived and a lowering of occupied anion-derived dangling-bond states, as compared to the ideal surface [8, 11].

The available self-consistent calculations of the nonpolar SiC(110) surface [11, 23] yield excellent mutual agreement concerning the surface atomic structure [7]. The optimized surface relaxation shown schematically in figure 1 is characterized by a bond-length-contracting rotation relaxation. The surface-bond-length contraction amounts to about 6% with respect to the SiC bulk-bond length [11, 23]. The relaxation angle ω results as 15.4° and 16.9° in [11] and [23], respectively. Thus, ω is much smaller at SiC(110) than at GaAs(110) where it amounts to some 30°. This difference is mainly due to the larger ionicity of SiC and to the more pronounced asymmetry of the charge density along the Si–C bonds, as compared to GaAs [11]. Concomitantly, the C anion in SiC is a first row element whose covalent radius is much smaller than that of the Si cation. In GaAs both ions have similar covalent radii. A full comparison of the optimized structure parameters resulting from *ab initio* calculations [11, 23] is given in [11], showing very good agreement for all parameters indeed. The relaxation-induced energy gain results as 0.64 and 0.63 eV per unit cell in [11] and [23], respectively.

The surface electronic structure of the relaxed SiC(110) surface is shown in the left panel of figure 2 together with the projected bulk-band structure (PBS). The calculated LDA gap is some 50% smaller than the experimental gap, as is usual in LDA results. In this and all the following figures of surface band structures the PBS is shown by shaded regions. The PBS exhibits an ionic gap between −8.5 and −10 eV, which is typical for ionic compound semiconductors. The relaxed surface gives rise to pronounced cation-(C_3) and anion-derived (A_5) surface-state bands within the gap-energy region. Their energetic separation is roughly

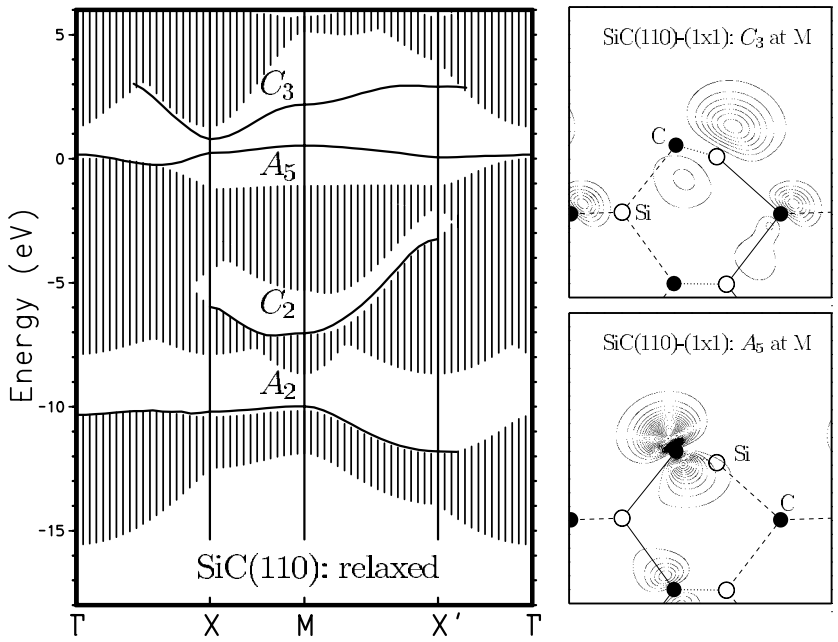

Figure 2. Surface band structure of the relaxed SiC(110)-(1 × 1) surface (left panel) and respective charge densities of the cation- and anion-derived dangling-bond states C_3 and A_5 at the M-point of the SBZ (right panels). The projected bulk band structure is shown by a vertically shaded area. Bonds within (parallel to) the drawing plane are shown by full (broken) lines. Bonds forming an angle with the drawing plane are shown by dotted lines (from [7, 11]).

0.2 eV. Thus, the nonpolar SiC(110) surface is obviously semiconducting. Additional anion- and cation-derived surface-state bands occur within the energy region of the projected bulk valence bands. The right panels of figure 2 reveal the origin and nature of the C_3 and A_5 dangling-bond states. Clearly, C_3 is a cation-derived (Si-derived) and A_5 is an anion-derived (C-derived) dangling-bond state. They are localized at the surface Si and C atoms, respectively. The surface electronic structure of the relaxed SiC(110)-(1 × 1) surface is very similar to that of the relaxed GaAs(110)-(1 × 1) surface (see [11]).

From a theoretical point of view, the surface structure of the relaxed SiC(110)-(1 × 1) surface can be considered as solved. To the best of our knowledge, this surface has not yet been investigated experimentally.

4. Polar SiC(111) surfaces

Polar SiC(111) surfaces have been studied using DFT-LDA calculations by Northrup and Neugebauer [27], Wenzien *et al* [42, 43], Furthmüller *et al* [44] and Starke *et al* [45]. The authors have investigated $1 \times 1, 2 \times 2$, $(\sqrt{3} \times \sqrt{3})$R30° and 3×3 reconstructions. Cubic 3C-SiC(111) surfaces are largely equivalent to respective hexagonal 6H-SiC(0001) surfaces (see [46]). Actually, low-energy electron diffraction (LEED), Auger electron spectroscopy (AES) and electron-energy loss spectroscopy (EELS) results are almost identical for corresponding reconstructions of the 3C-SiC(111) and the 6H-SiC(0001) surfaces [47] since the stacking sequence of Si-C bilayers in the cubic [111] direction of 3C-SiC and in the hexagonal [0001] direction of 6H-SiC are identical down to the fourth bilayer, i.e. down to

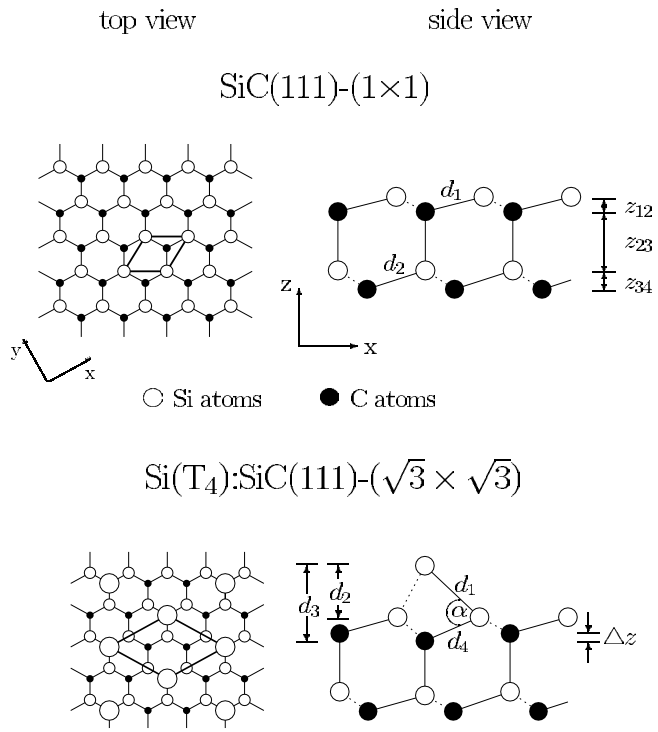

Figure 3. Top panels: top and side view of the relaxed Si-terminated 3C-SiC(111) surface. Bonds lying in the drawing plane or parallel to it are shown by full lines and those forming an angle with the drawing plane are shown by broken lines. Bottom panels: top and side view of the optimized $\sqrt{3}\times\sqrt{3}$ R30° reconstruction of the Si-terminated 3C-SiC(111) surface. The surface is terminated by Si adatoms in T_4 positions. The 1×1 and $\sqrt{3} \times \sqrt{3}$ unit cells are indicated by heavy lines in the left panels, respectively. Si and C atoms are shown by open circles and full dots, respectively. The actual values of the structure parameters are compiled in [29].

the eighth atomic layer. Based on the indistinguishable LEED results for these two surfaces one can conclude that they are characterized by the same reconstruction geometry. Among the structures reported are 1×1, $(\sqrt{3} \times \sqrt{3})$R30°, 3×3, $(6\sqrt{3} \times 6\sqrt{3})$R30° and 9×9 configurations depending sensitively on temperature and sample preparation [46–53]. Many experimental results on hexagonal SiC surfaces have been collected by Starke [46]. In view of the equivalence of 3C-SiC(111) and 6H-SiC(0001) surfaces, theoretical results on the latter apply equally well to the former. Nevertheless, we will dwell on polar hexagonal (0001) surfaces only to the extent that is needed to illustrate basic structural and electronic properties of 3C-SiC(111) surfaces.

4.1. Relaxed SiC(111) surfaces

The structure of the relaxed Si- and C-terminated 6H-SiC(0001)-(1×1) and the relaxed Si-terminated 3C-SiC(111)-(1×1) surfaces has been optimized by Sabisch *et al* [29] and by Wenzien *et al* [43], respectively. In these calculations only very small inward relaxations of the top Si (-0.25 Å [29], -0.06 Å [43]) or C (-0.15 Å [29]) layers are found in good general agreement with LEED data [54]. A top and a side view of the lattice structure for the Si-terminated surface are shown in the upper panels of figure 3. For the C-terminated surface,

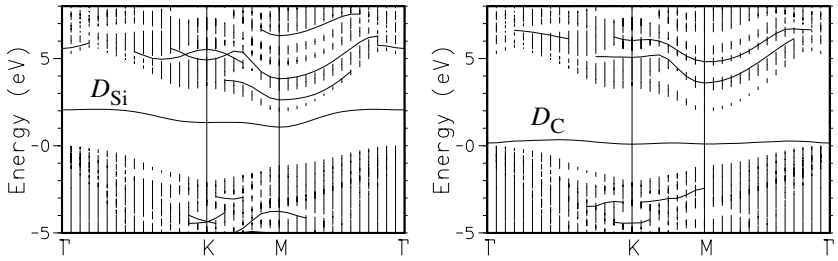

Figure 4. Surface band structures of the relaxed Si-terminated (left panel) and C-terminated (right panel) 6H-SiC(0001)-(1 × 1) surfaces (from [29]).

the relaxation-induced energy gain is 0.30 eV per unit cell [29]. For the Si-terminated surface, the DFT-LDA calculations agree, finding an energy gain of 0.10 or 0.09 eV per unit cell, [29] and [43], respectively.

The electronic structure of the relaxed Si- and C-terminated surfaces shows one dangling-bond band within the projected gap in each case (see figure 4). These bands originate from the dangling bonds which are localized at the Si or C top layer atoms, respectively. At the Si- or C-terminated surface the band resides in the upper or lower part of the gap, respectively [29]. Since there is only one top-layer atom per unit cell in both cases (see figure 3) with one electron that is not used for binding the top layer atom to the three nearest neighbours on the second layer, the dangling-bond band is only half-filled in each case so that the surfaces are metallic. In principle, they can reduce the number of unsaturated dangling bonds by reconstruction. In general, one would expect the surfaces thereby to become semiconducting.

4.2. Reconstructed SiC(111) surfaces

Contrary to many other semiconductor surfaces, the single-particle band structures of most of the cubic 3C-SiC(111) or hexagonal 6H-SiC(0001) surfaces do not become semiconducting upon reconstruction. This is due to the fact that, for all odd $n \times m$ reconstructions with $n \cdot m$ odd, such as the 1×1, $(\sqrt{3} \times \sqrt{3})$R30°, 3×3, $(6\sqrt{3} \times 6\sqrt{3})$R30° and 9×9, the number of atoms per surface unit cell is odd, therefore leading to a half-filled uppermost band in the one-particle spectrum and a metallic surface. Only if the reconstruction is even, with $n \cdot m$ being an even integer, such as 2×1 or 2×2, can a fully occupied uppermost surface valence band separated by a gap from the lowest surface conduction band arise. Nevertheless, odd reconstructions of 3C-SiC(111) and 6H-SiC(0001) have also been identified experimentally as semiconducting (see [55–59]). These experimental results can be interpreted by taking into account electronic correlation effects in the calculations [13, 44, 60, 61] lending strong support to a Mott–Hubbard picture of these SiC surfaces. This topic is addressed in detail elsewhere in this issue [62].

4.2.1. SiC(111)-(2 × 2). Wenzien *et al* [43] have theoretically studied various 2×2 reconstructions of a Si-rich 3C-SiC(111) surface. They obtained a significant energy lowering, as compared to the 1×1 surface, for a 2×2 vacancy-buckling model very similar to respective models of cation-terminated GaAs(111) or ZnSe(111) surfaces. The model exhibits s-like dangling bonds at the C atoms which are filled with two electrons and Si p-like dangling bonds which are empty. This model appears to be semiconducting in accord with the above general assessment. To the best of our knowledge, this reconstruction has not been observed experimentally to date.

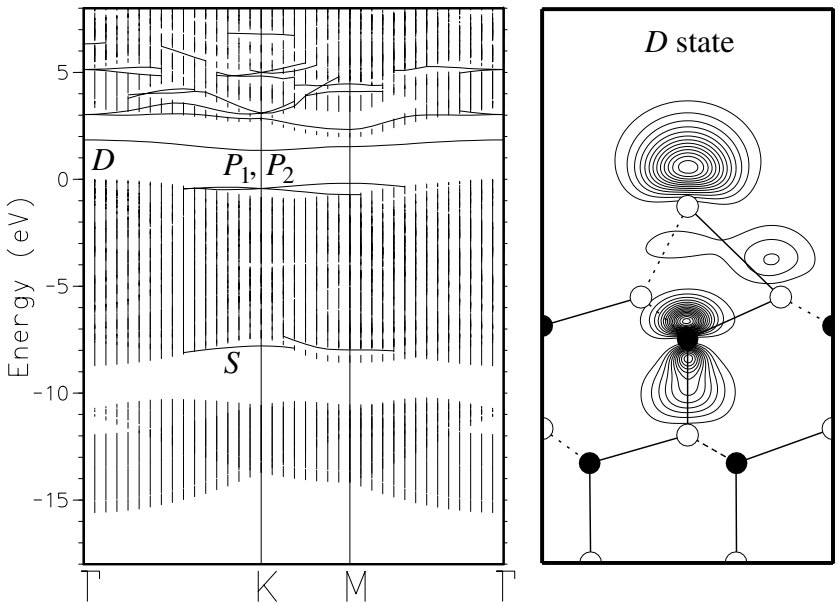

Figure 5. Surface band structure of the Si-terminated 6H-SiC(0001)-($\sqrt{3} \times \sqrt{3}$)R30° surface for Si adatoms in T_4 position (see lower panels of figure 3) and charge–density contour of the salient surface dangling-bond state D at the M point of the SBZ.

4.2.2. SiC(111)-($\sqrt{3} \times \sqrt{3}$)*R*30°. Most models of the cubic or the equivalent hexagonal $\sqrt{3}$ reconstruction involve Si or C adatoms at the substrate surface. They are therefore called adsorption-induced reconstructions. A whole variety of adatom configurations has been investigated by first-principles calculations [13, 27, 29, 44]. It has turned out that at the Si-rich surface 1/3 of a Si monolayer with the adatoms in T_4 positions (see lower panels of figure 3) yields by far the lowest grand canonical potential for all allowed values of the Si chemical potential [27, 29]. The Si (T_4) adatom structure of the $\sqrt{3}$ surface has been experimentally solved more recently by grazing incidence x-ray diffraction (GIXRD) [63]. Very good agreement between the calculated optimal surface structure and the GIXRD data was found. In recent years, the Si (T_4)$\sqrt{3}$ structure, which can be formed easily by heating the samples, has been investigated intensively in experiment by, for example, direct angle-resolved (ARPES) and angle-resolved inverse photoelectron spectroscopy (ARIPES) [55–58], EELS [59] and STM [64] measurements. The DFT-LDA band structure for this surface results in very good general agreement from the different calculations [27, 29, 44]. It is shown in figure 5 together with the charge density of the most prominent Si dangling-bond state D. In the T_4 configuration the Si adatoms saturate the three dangling-bond orbitals of the Si substrate top layer atoms. The adatoms, in turn, give rise to one new dangling-bond orbital containing one unpaired electron per unit cell. In the single-electron picture this one electron per unit cell leads to a half-filled surface dangling-bond band D in the projected gap so that the LDA surface band structure is again metallic. But the ARPES and ARIPES [55–58], EELS [59] and STM [64] data clearly reveal a fully occupied and an entirely empty dangling-bond band in the gap showing that the surface is semiconducting. These findings can also be interpreted within the Mott–Hubbard picture mentioned above [13, 44, 60, 62], yielding excellent agreement between the calculated lower and upper Hubbard bands and the measured occupied and empty surface state bands in the gap (see [13]).

4.2.3. SiC(111)-(3 × 3). The structure of the reconstructed 3 × 3 surface has been investigated employing STM, LEED and LEED holography experiments, as well as DFT-LDA calculations [45]. A structure consisting of Si tetramers on a twisted Si adlayer (the adcluster/adlayer model) was found to be the optimal structural model. Investigations of the electronic structure of this surface by ARPES measurements and DFT-LDA calculations [44] show that also in this case DFT-LDA yields a metallic surface while ARPES data indicate no density of states (DOS) at the Fermi level. This discrepancy can also be resolved within the Mott–Hubbard picture [44]. These findings are convincingly corroborated by more recent ARPES and ARIPES [65], as well as EELS [59] data. Nevertheless, the agreement between experiment and theory is not entirely conclusive, as yet. Other reconstructions, such as the Kulakov model [66], might show similar occupied and empty surface state bands within the gap when electronic correlation is taken into account [44], as argued by Johansson *et al* [65].

5. Polar SiC(001) surfaces

Bulk-truncated polar SiC(001) surfaces are nominally terminated either by a single silicon or carbon layer with one Si or one C atom per surface unit cell, respectively. Therefore, we refer to these surfaces as Si-terminated or C-terminated SiC(001) or, in short, as Si face and C face, respectively. In the *ideal* 1 × 1 configuration the surface atoms have two broken sp^3 bonds in each case. These dehybridize at the geometrically *ideal* surfaces by electronic relaxation forming one s, p_z dangling bond and one p_x, p_y bridge bond [12]. *Real* SiC(001) surfaces show 1 × 1, 2 × 1, c(2 × 2), c(4 × 2), 3 × 2, 5 × 2, 7 × 2 and $n \times 2$ ($n \geqslant 8$) reconstructions (see [4, 10]), depending very sensitively on surface preparation conditions and surface stoichiometry. Kaplan [47] and many other authors [67–84] have shown that the different surface reconstructions of SiC(001) can reversibly be changed with Si coverage by an appropriate choice of sample temperature and Si flux in surface preparation. Increased Si flux and decreased temperature augment the Si concentration while increased temperature or annealing in vacuum leads to a Si depletion. The sequence of superstructures can reversibly be changed, as well, by exposure of Si_2H_6 or C_2H_2 [74]. The numerous superstructures of SiC(001) have been investigated in experiment in great detail using combinations of LEED, AES, EELS, STM, XPS, UPS, ARPES, ARIPES, near-edge x-ray absorption fine structure (NEXAFS) measurements, core-level spectroscopy (CLS) and medium energy ion scattering (MEIS). All experimental results agree that the c(2 × 2) reconstruction occurs at the C face while all other reconstructions occur at clean or Si-covered Si faces. For quite some time the origins of different reconstructions of SiC(001) surfaces have been discussed in terms of respective Si(001) and C(001) surfaces. However, this is inappropriate in many cases, as will be described in detail below. Here we only mention that the diamond (001) surface does not show a c(2 × 2) but only a very stable 2 × 1 reconstruction and the Si(001) surface does not show 3 × 2, 5 × 2, 7 × 2 or $n \times 2$ reconstructions with $n \geqslant 8$ but only 2 × 1 and c(4 × 2) reconstructions (see [8]). Actually, the reconstructions of the C and Si face of SiC(001) are very different as well. For *stoichiometric* surfaces, the energy gain due to reconstruction with respect to ideal 1 × 1 surfaces is of the order of 5 eV per surface unit cell at the c(2 × 2) C face while it amounts to only some 10 meV per surface unit cell at the clean 2 × 1 Si face. This is related to the fact that the forces needed to bend sp^3 bonds at C atoms are much larger than those at Si atoms. As a consequence, C atoms can easily move towards each other above the Si layer and form strong dimer bonds, as opposed to Si atoms above the C layer. The different widths of the bulk phonon spectra of diamond (165 meV), SiC (121 meV) and Si (64 meV) can be considered as a measure for the respective bond bending forces.

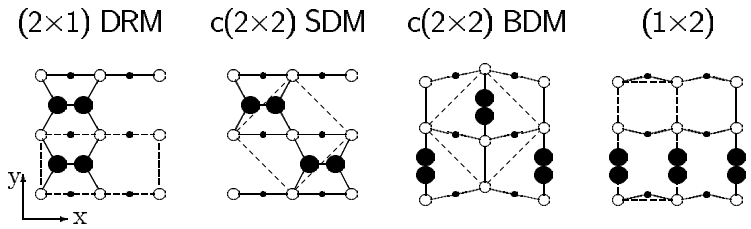

Figure 6. Top views of the 2 × 1 dimer-row, the c (2 × 2) staggered-dimer, the c(2 × 2) bridging dimer and the (1 × 2) C≡C dimer-row configurations of the C-terminated SiC(001) surface. The unit cell is indicated by broken lines in each case (from [12]).

In this section, we first address reconstruction models that have been investigated for the C-terminated surface and then discuss in more detail the fairly intricate reconstructions of stoichiometric and nonstoichiometric Si-terminated surfaces.

5.1. C-terminated SiC(001) surface

Four reconstruction models for the C face of SiC(001) have been discussed widely in the literature. They are characterized by double- or triple-bonded carbon dimers at the surface (see figure 6). Their atomic configurations derive from a bulk-truncated lattice with the top layer C atoms moving closer together into new equilibrium positions at the free surface. Since the lattice constant of SiC is 22% larger than that of diamond and the covalent radius $r_C = 0.77$ Å of the C anions is very small such atomic movements can easily take place without inducing strong Coulomb repulsions with the back bonds. When top layer C atoms move laterally towards each other double-bonded C=C dimers can easily form, very much like at the C(001)-(2 × 1) surface [85]. Alternatively, carbon dimers may form in the surface layer, bridging two Si atoms on the second layer. In this case, the top layer carbon atoms can come even closer together and form triple-bonded C≡C dimers. The respective mechanism does not occur at the C(001)-(2 × 1) surface since the lattice constant of diamond is too small to allow for C≡C triple-bonded dimers bridging second layer C atoms in that case. Distributing the double- or triple-bonded dimers in rows or in staggered arrangements yields the four distinctively different reconstruction models shown in figure 6. While each of them gives rise to a very pronounced lowering in the total energy with respect to the ideal surface (more than 4.5 eV per dimer or surface unit cell, respectively) they are fairly close in total energy with respect to one another. This has made the theoretical determination of the optimal structure a demanding task.

A number of DFT-LDA structure optimizations, carried out in the mid-1990s [12, 24–26, 28], has yielded results for the different models which are in very good general accord with one another. From the calculations the following picture emerges. The 2 × 1 dimer-row model (DRM) is characterized by rows of C=C dimers. Their bond length of 1.36 Å is very close to the C=C double-bond length of 1.37 Å in molecules, such as C_2H_4. When these dimers are distributed in a staggered configuration the resulting c(2 × 2) staggered-dimer model (SDM) again yields a C=C double-bond length of 1.36 Å. The c(2 × 2) bridging-dimer model (BDM) is characterized by C≡C dimers, bridging two Si atoms in the sublayer, with a bond length of 1.22 Å which is typical for carbon triple bonds in hydrocarbon molecules. In the BDM, the C≡C dimers are distributed in a staggered configuration, as shown in figure 6. For example, in our LDA calculations [12] for the c(2 × 2) BDM a reconstruction-induced energy gain of 4.76 eV per dimer is obtained which is only 0.03 eV larger than that for the SDM (4.73 eV) but 0.12 eV smaller than that for the DRM (4.88 eV). Finally, the 1 × 2 structure in figure 6 is characterized by C≡C dimer rows with a dimer-bond length of 1.22 Å, as well. The latter model

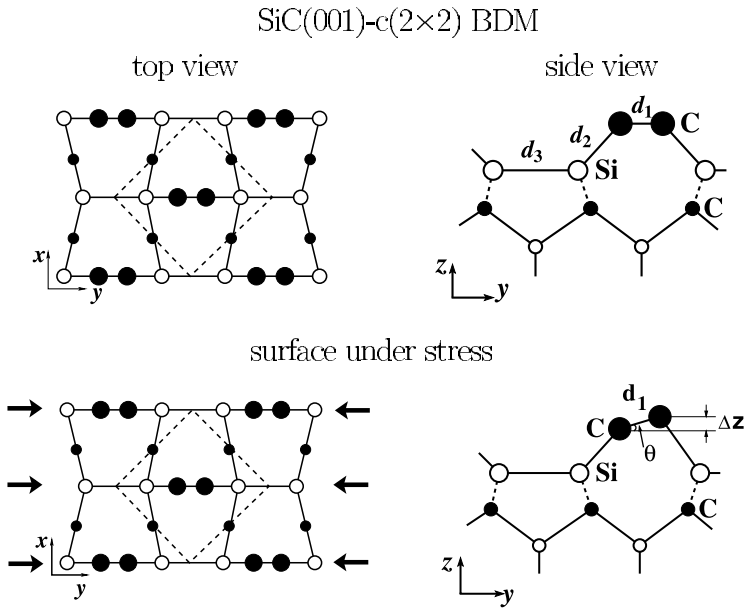

Figure 7. Upper panels: top and side views of the BD model for the C-terminated SiC(001)-c(2×2) surface. Lower panels: top and side views of the optimized atomic structure of the BDM under stress. The filled (open) circles represent carbon (Si) atoms and the size of the circles decreases from surface to bulk. The unit cell is indicated by broken lines in the left panels (from [93]). Note that the top views of the BDM are rotated by 90° with respect to figure 6 to allow for more clear plots of the side views.

yields the smallest energy gain of 4.58 eV so that it turns out to be the least favourable of the four models. Thus DFT-LDA calculations find the c(2 × 2) BDM to be slightly lower in energy than the c(2 × 2) SDM but the most stable configuration resulting from these calculations is the 2 × 1 DRM.

Experimentally, however, a c(2 × 2) reconstruction is observed (see [70]). Bermudez and Kaplan [49] have suggested a structural model for the c(2 × 2) reconstruction based on an arrangement of staggered carbon dimers. The C atoms in these dimers are sp^3-hybridized, each with σ bonds to the two nearest-neighbour Si atoms on the second layer and a σ bond to the neighbouring C atom in the surface dimer. This would be a SDM, as shown in figure 6. Based on their LEED results, Powers *et al* [71] proposed the bridging-dimer model (BDM in figure 6). The BDM is also strongly supported by experimental results of NEXAFS measurements by Long *et al* [86]. Also, Yeom and co-workers [87–90] have reported detailed investigations of the SiC(001)-c(2 × 2) surface confirming the BD model. Employing STM, surface-core-level-resolved photoelectron diffraction (PED) and angle- as well as polarization-resolved PES, the authors find the surface to uniquely and uniformly consist of anomalously triple-bonded C≡C dimers. The filled-state STM images recorded by Yeom *et al* clearly show a staggered c(2 × 2) reconstruction with symmetric C≡C dimers confirming the BD reconstruction. A top and a side view of the BDM specifying the most important structural parameters is shown in the top panels of figure 7. Yeom *et al* determined a C≡C dimer-bond length of $d_1 = 1.22 \pm 0.05$ Å. The nearest-neighbour distance between the C dimer atoms and Si sublayer atoms was found to be $d_2 = 1.84 \pm 0.02$ Å and the distance of the Si atoms in the sublayer was determined to be $d_3 = 2.70 \pm 0.1$ Å. In addition, these authors carried out detailed angle- and polarization-resolved PES studies to investigate the electronic structure of

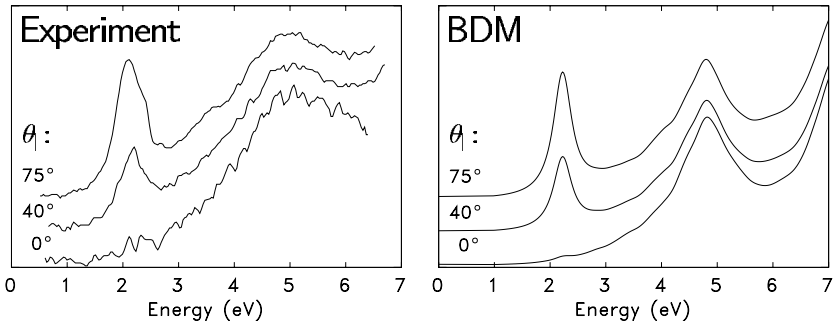

Figure 8. Experimental NEXAFS spectra from [86] in comparison with calculated NEXAFS spectra for the BDM [95].

the BDM, yielding a considerable number of surface state bands and resonances. Most recently, Derycke *et al* [91] have investigated the SiC(001)-c(2 × 2) surface by STM measuring both filled and empty electronic states. From the filled-state STM image, the C≡C dimers appear to be symmetric. Surprisingly, the empty-state STM images show an asymmetry between the two C atoms of each surface dimer. The observed differences in the vertical atomic positions of the two C dimer atoms range from 0.07 to 0.1 Å. On the basis of these findings, Derycke *et al* claim the existence of *asymmetric* dimers at their SiC(001)-c(2 × 2) samples which were assumed to be under surface stress.

The above results clearly reveal that experiment strongly supports the c(2 × 2) BD model while LDA calculations slightly favour the 2 × 1 DR model. Now it is known that LDA calculations may be inappropriate to describe the relative energetics of C=C versus C≡C dimers accurately enough. Therefore, more refined DFT calculations [92, 93] have recently employed the GGA in addition to the LDA. In perfect agreement with experiment, both GGA studies yield a reversed energetic ordering of the c(2 × 2) BD and 2 × 1 DR reconstruction, as compared to the LDA results. At the bulk theoretical lattice constant, the BD model is found to be lower in energy by 0.25 or 0.29 eV per dimer, [92, 93] respectively, as compared to the 2 × 1 DR model and 0.3 eV lower than the c(2 × 2) SD model [93]. Most recently, an additional GGA structure optimization has been reported [94], which also finds the BDM to be the optimal surface structure. In all three GGA calculations [92–94] the carbon dimers in the BDM result as symmetric.

The most important structure parameters of the BD model, as resulting from the *ab initio* LDA and GGA calculations are compiled in table 1. All calculations for the stress-free surface yield symmetric C≡C surface dimers. It is very gratifying to see how well the results of current *ab initio* calculations of the structure of this surface agree with one another and with experiment. There is one very interesting difference between experiment and theory to be noted, however. While the bond length of the second layer Si dimers results roughly as $d_3 = 2.40$ Å from all calculations, experiment observes a value of 2.70 Å. This discrepancy still remains to be unravelled.

Figure 8 shows NEXAFS spectra for the electric field vector parallel to the dimer direction, as recorded by Long *et al* [86] in comparison with calculated spectra [95] for the bridging-dimer model. It is most obvious from the figure that the calculated spectra for the BDM are in excellent agreement with the measured spectra. This is not at all the case for the spectra of the SDM (not shown in figure 8 for brevity's sake). The agreement between the measured NEXAFS spectra and those calculated for the BDM yields an additional convincing confirmation of the bridging-dimer model.

Table 1. Optimized structure parameters (as defined in the upper right panel of figure 7) for the BD model of the C-terminated SiC(001)-c(2 × 2) surface from a number of *ab initio* calculations and from experiment [89, 90].

	LDA [12]	LDA [25]	LDA [26]	LDA [28]	GGA [92]	LDA [93]	GGA [93]	GGA [94]	EXP [89, 90]
d_1 (Å)	1.22	1.23	1.22	1.23	1.25	1.22	1.23	1.23	1.22 ± 0.05
d_2 (Å)	1.83	1.82	1.87	1.81		1.82	1.85	1.85	1.84 ± 0.02
d_3 (Å)	2.40	2.38	2.38	2.37	2.42	2.39	2.42	2.42	2.70 ± 0.10

Strong further support for the BDM is obtained from the surface electronic structure, shown in figure 9. It has been calculated recently [93], employing potential scattering theory [32, 39, 40] to clearly identify the many surface resonances in addition to the bound states. Obviously, the c(2 × 2) BDM is semiconducting. There are neither occupied nor empty surface states in the gap. This is in good accord with earlier PES measurements by Bermudez and Long [96], as well as with more recent ARPES [89] and ARIPES [97] data. The lack of occupied or empty surface states in the fundamental gap originates from the fact that there are no unsaturated C dangling bonds at the surface of the BDM. The calculated occupied (T_1–T_8) and empty ($T_1^\star$–$T_3^\star$) bands and the experimentally observed surface state bands from ARPES [89] and ARIPES [97] measurements show a lot of good agreements. It should be noted that no ARPES or ARIPES data have been reported along the S′–M and M–S lines of the SBZ. The other reconstruction models (see figure 6), whose surface band structure has been discussed in detail in [6, 8, 12, 24, 25], do not show satisfying agreement with the data. The c(2 × 2) SDM, in particular, yields a metallic surface band structure with a number of occupied and empty surface state bands in the gap energy region in contradiction to the ARPES and ARIPES data [89, 97]. There is also no clear indication of surface states in the bandgap in EELS data (see [4, 47]). Only *H*-sensitive structure has been observed in EELS at about 4 eV and between 8 and 11 eV which is clearly due to surface excitations [49]. The EELS peak at about 4 eV could originate from $T_1 \rightarrow T_1^\star$ transitions (taking into account a quasiparticle gap correction of about 1 eV [12]). The other features between 8 and 11 eV might well be related to the many possible transitions between the surface state bands within the projected valence and conduction bands in figure 9. The origin, character and symmetry properties of the surface-induced bound states and resonances has been discussed in detail in terms of charge–density distributions of all salient surface features in [93]. Not only energy positions and dispersions but also the symmetry properties of a number of calculated bands shown in figure 9 have been found to be in very good accord with the ARPES data [89].

On the basis of the recent *ab initio* calculations [92–94], as well as a whole body of experimental data [71, 86–91, 97], there is now general agreement that triple-bonded C≡C dimers form the main building block of the BD reconstruction of SiC(001)-c(2 × 2). Nevertheless, there remains the question whether these dimers are symmetric, as resulting from all calculations for the stress-free surface, or buckled, as suggested by Derycke *et al* [91] on the basis of their STM measurements. For occupied states, these authors obtain symmetrically shaped height profiles with one peak in each surface unit cell while the empty state topographs show two asymmetric peaks with a different height within each unit cell. Based on these findings the authors postulate the existence of asymmetric dimers at the c(2 × 2) surface. As the driving force for the asymmetric dimer reconstruction they suggest compressive stress along the dimer direction. The effect of surface stress on the BDM has been studied recently by *ab initio* calculations [93]. It turns out that compressive stress along the dimer direction (see lower panels of figure 7) leads to an asymmetric tilt of the dimers. The lengths of the

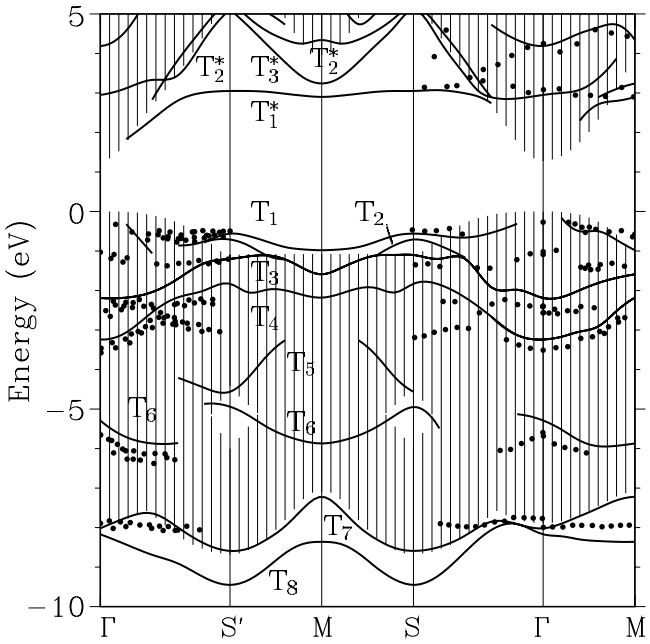

Figure 9. Surface band structure of the BDM of the C-terminated SiC(001)-c(2 × 2) surface (from [93]) in comparison with ARPES [89] and ARIPES [97] data.

dimer bond and the C–Si back bonds remain basically unchanged by the applied stress so that the angle θ between the dimer-bond direction and the surface plane increases when the lattice constant in the dimer direction is decreased. The electronic structure of the c(2 × 2) surface under stress (see figure 5 in [93]) is similar to the one shown in figure 9 for the unstrained case except for some small energy shifts of some bands. The agreement of the calculated bands with the measured bands slightly improves in a few cases, most noticeably for the bands T_4, T_6 and T_7. A comparison of the ARPES data [89] with the calculated surface band structure for both the unstrained, as well as the strained lattice, yields reasonable agreement in both cases [93]. The small differences in the electronic structure for the two configurations do not allow us to clearly rule out either one with respect to the other.

Figure 10 shows STM images for the c(2 × 2) surface compressed by 7% in the dimer direction (see lower part of figure 7) which have been calculated employing the Tersoff–Hamann approach [41]. The resulting images in the constant current mode are shown in the upper panels for filled states near the valence band maximum (upper left) and for empty states near the conduction band minimum (upper right). In addition, height profiles from X to X′ as calculated [93] (middle panels) and measured [91] (bottom panels) are shown for further comparison. The filled-state image (upper left) shows only slightly asymmetric spots. The regions near the C up-atoms are somewhat brighter than the ones near the C down-atoms in the dimers. The calculated height profiles (broken lines in the middle panels) have been broadened by 0.5 Å to take the finite size of the tip into account. The resulting filled-state profile, shown as a full line in the left middle panel of figure 10, has practically a symmetrical shape. In contrast, the calculated image for the empty states (upper right panel) shows distinctly asymmetric spots, each of which is separated by a nodal line in the direction perpendicular to the dimers. The regions around the up-atoms are distinctly brighter than the regions around the down-atoms of the C≡C dimers. This can be seen more clearly in the profile from X to

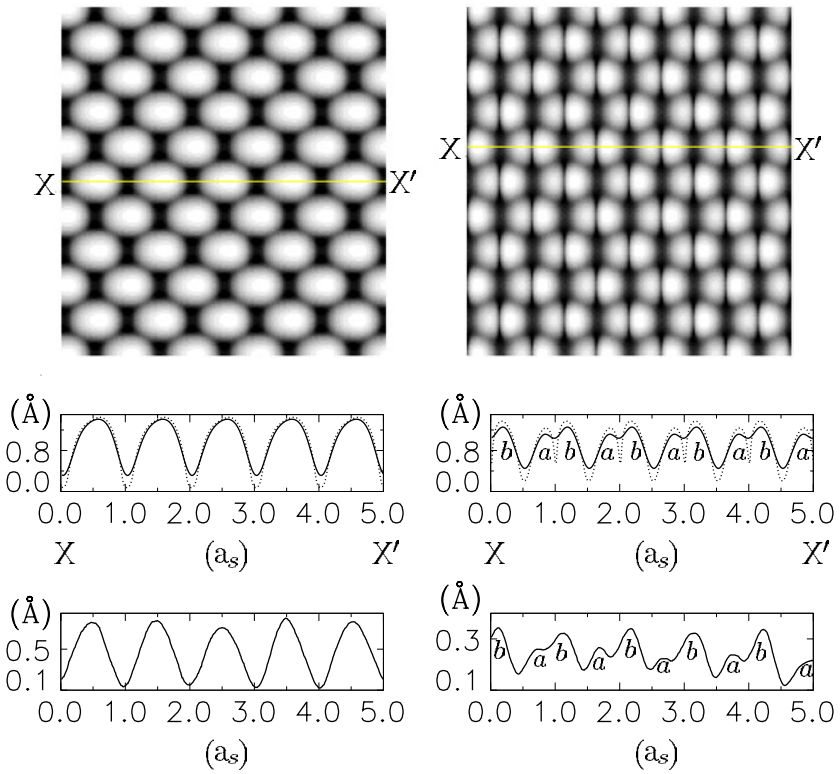

Figure 10. Calculated STM images for filled and empty states at the compressed SiC(001)-c(2 × 2) surface (left and right top panels, respectively). States with a constant charge density of 0.00032 e au^{-3} are plotted. The calculated height profiles along X–X′ are shown as dotted lines in the middle panels. The corresponding full lines are obtained by broadening the height profiles (see the text). Experimental height profiles along X–X′ from [91] are shown for filled and empty states (left and right bottom panels, respectively) for comparison (from [93]).

X′ along the dimer direction (middle right panel) in which the nodal lines manifest themself as distinct minima. Also the broadened topographs show a significant asymmetry. Thus, a slightly asymmetric configuration of the C≡C surface dimers as resulting from compressive stress gives rise to filled-state STM images which look distinctly different from empty-state images. The height profiles originating from filled electronic states have basically a symmetric shape so that one would not expect to find any asymmetry in the profiles from filled states in STM measurements. This conclusion is borne out by the experimental height profiles in the lower left panel of figure 10. On the other hand, the calculated empty-state topographs are clearly asymmetric in satisfactory agreement with the experimental findings (see lower right panel of figure 10). These results qualitatively support the structural model worked out by Derycke *et al* [91] for the SiC(001)-c(2 × 2) surface. Quantitatively, however, there are differences in the relative height of the two peaks between the calculated and measured STM profiles. These deviations may partly be traced back to a limited accuracy of the basis set used in the calculations representing the wavefunction far outside the crystal in the region of the STM tip. In conclusion, the calculated STM topographs in figure 10 allow us to rationalize the experimental findings of symmetrically and asymmetrically shaped height profiles for the occupied and empty states, respectively, when surface stress is invoked [91, 93]. In spite of this

good qualitative agreement, we would like to stress, however, that many previous experiments have observed symmetric C≡C dimers at the surface [71, 86–90, 97] and that Yeom *et al* [89] have successfully interpreted the results of their STM, PED and ARPES investigations on the basis of a surface configuration with symmetric dimers. It is worthwhile to remember in this context that SiC is a material which exists in a large number of polytypes with different structural modifications. It may thus be possible that the SiC(001)-c(2 × 2) surface exhibits symmetric, as well as, asymmetric dimers depending on details of sample preparation. Further investigations seem necessary to clarify this remaining question concerning the BD model of the SiC(001)-c(2 × 2) surface.

5.2. Si-terminated SiC(001) surfaces

As noted above, the Si face shows a very rich variety of 2 × 1, c(4 × 2), 3 × 2, 5 × 2, 7 × 2, 8 × 2 and 15 × 2 surface reconstructions, depending on preparation conditions and surface stoichiometry. This is certainly related to the fact that the relatively extended Si orbitals reside on a comparatively small two-dimensional lattice at the SiC surface. As a consequence, a very detailed energetic balance needs to be met for stability, giving rise to the large number of competing metastable structures. They belong to the most intricate and most intensively studied reconstructions of the SiC polytypes. The numerous preparation procedures described in the literature vary in a number of subtle details but have many important steps in common (see [4, 47, 67–84]). Mostly, thin SiC films of a few micrometres thickness, grown on Si(001) substrates by chemical vapour deposition (CVD), are used at the outset. In a few cases SiC epilayers, grown by molecular beam epitaxy (MBE) on such samples, have been employed, as well. Nominal Si(001) substrates or, preferentially, intentionally miscut or misoriented Si(001) substrates are being used. The latter technique has the important advantage to yield single-domain surfaces. The samples are first outgassed or outbaked and in a next step the natural oxide is removed by heating at 950–1050 °C in a Si flux. Depending on temperature, heating time and total Si exposure, samples with 3 × 2, 5 × 2, 7 × 2, c(4 × 2) and 2 × 1 reconstructions have been prepared in order of decreasing Si coverage and could be changed reversibly. Auger experiments on the $(Si_{LVV})/(C_{KLL})$ peak-to-peak height ratios [70, 76] show that the amount of Si atoms at the Si-terminated SiC(001) surface increases according to the following relations: $2 \times 1 \cong c(4 \times 2) < 7 \times 2 < 5 \times 2 < 3 \times 2$, with the 3 × 2 being fully Si saturated, i.e. an ordered structure with the largest possible Si coverage. Hara *et al* [75, 76] and Shek [77] have observed a 7 × 2 phase between the c(4 × 2) and 5 × 2 phases and Douillard *et al* [98] and Kitamura *et al* [81] have observed 8 × 2 and 15 × 2 reconstructions between 3 × 2 and 5 × 2 phases, respectively. By additional heating without Si flux at about 1000–1150 °C, the Si-rich 3 × 2 and 5 × 2 phases could be transformed into 2 × 1 and c(4 × 2) structures [47, 77, 78, 80, 82, 99]. Hüsken *et al* [100] were also able to realize this transformation to the 2 × 1 reconstruction, but the authors could not observe a c(4 × 2) reconstruction, neither on their CVD- nor on their MBE-grown samples. It had been found previously that the c(4 × 2) reconstruction was rather difficult to show probably because of surface roughness or contamination (see [4, 47]). Using the preparation procedure indicated above, Shek [77] observed a c(4 × 2)* reconstruction showing strong c(4 × 2) and very weak 2 × 2 LEED spots. Soukiassian and co-workers nowadays routinely obtain very reproducible and clean c(4 × 2) surfaces by annealing clean and well-ordered 3 × 2 samples at 1150 °C [10, 80, 83, 101, 102]. Using a few more preparation steps going through the c(2 × 2) C face and including atomic layer epitaxy, Duda *et al* [84] have also achieved well-prepared c(4 × 2) reconstructions in recent years. Further annealing of their c(4 × 2) samples or leaving them for several hours in the UHV system led to 2 × 1 surfaces.

In general, all authors obtain a well-defined Si-rich 3×2 reconstruction when annealing the samples at 900–1100 °C under Si flux for an appropriate time. The 3×2 surface, therefore, appears to be the most stable surface configuration under Si-rich preparation conditions. For Si-poor conditions, e.g. realized by further annealing the 3×2 surface at 1000–1150 °C without Si flux, first a 5×2 and then a $c(4 \times 2)$ or a 2×1 reconstruction is observed. From the experimental evidence it appeared for quite some time that the 3×2, 5×2 and 2×1 reconstructions could readily be prepared while the $c(4 \times 2)$ reconstruction was more complicated to arrive at. Actually, even today, there is an ongoing discussion related to the correspondence between the 2×1 and the $c(4 \times 2)$ surface. Shek [77] considered the 2×1 surface as the low coverage limit of a $c(4 \times 2)$ surface while Soukiassian and co-workers [10, 80, 83, 101, 102] concluded that the 2×1 surface at room temperature is a 'failed' $c(4 \times 2)$ surface driven by defects or impurities. The latter authors have observed [101] a reversible structural phase transition near 400 °C between the $c(4 \times 2)$ and the 2×1 phase accompanied by a semiconductor–metal transition. The latter conclusion has been questioned recently by Duda *et al* [84] on the basis of their ARPES data showing that both phases are semiconducting. Finally, we note that Hara *et al* [70] have interpreted the $c(4 \times 2) \leftrightarrow 2 \times 1$ transition as an order–disorder phase transition.

Many experimental investigations come to the conclusion that the 2×1 and the $c(4 \times 2)$ surfaces are terminated by one complete Si atom layer (see [47, 67, 70, 82, 84, 103]), while Shek [77] concluded a coverage of about two monolayers since his soft x-ray Si 2p core-level spectra could not be reconciled with a single Si layer termination of the $c(4 \times 2)$ surface. Concerning the 5×2 and 3×2 structures, all experimental data agree that they are covered by an ordered partial Si overlayer on top of the Si face. However, the actual Si coverage in the adlayer of these two reconstructions is still a matter of controversial debate. The different preparation cycles mentioned above reveal that there is a close correspondence between the different reconstructions of the Si face. This seems to be particularly true for the closely related 2×1 and $c(4 \times 2)$ surfaces. Thus, when we focus in the following discussion on different reconstructions one at a time, for clarity's sake, one should bear in mind that there are interesting interrelations between all of them.

We have investigated the ideal 1×1 surface and the $2 \times 1, c(4 \times 2), 3 \times 2$ and 5×2 reconstructions by *ab initio* LDA calculations and have suggested reconstruction models following from minimum surface formation energy in each case. They will be discussed in comparison with experiment and other pertinent theoretical work in the following subsections. Certainly, it is still an open question whether our models are fully appropriate. But since they follow as minimum grand canonical potential structures from calculations carried out on an equal footing for all reconstructions, it seems meaningful to address their relative formation energies for Si-poor and Si-rich preparation conditions already at this point. The formation energies $\Delta\Omega$ of the $c(4 \times 2)$, the 5×2 and the 3×2 reconstructions, i.e. the difference in grand canonical potential of a particular reconstruction and the total energy of the ideal 1×1 surface, are shown in figure 11. To check whether the 3×2 structure with $\Theta_{Si} = 2$ is the fully Si-saturated surface, the case $\Theta_{Si} = 2 + 1/3$ has also been considered (see figure 11). Clearly, for Si-poor preparation conditions (curve (a)), the $c(4 \times 2)$ model has the lowest formation energy while for Si-rich growth conditions (curve (b)), the 3×2 model has the lowest formation energy. The formation energy of the 5×2 model lies in both cases in between those of the 3×2 and the $c(4 \times 2)$ models. These results are in very good general accord with the experimental growth results summarized above. In the Si-rich case, i.e. for $\mu_{Si} = \mu_{Si(bulk)}$, the 3×2 surface is clearly the most stable. Reducing its Si coverage by annealing without Si flux, the surface is expected to first transform into a 5×2 and then into a $c(4 \times 2)$ surface with decreasing Si coverage. For Si-poor conditions, i.e. for $\mu_{Si} = \mu_{Si(bulk)} - \Delta H^{f}_{SiC}$, on the other

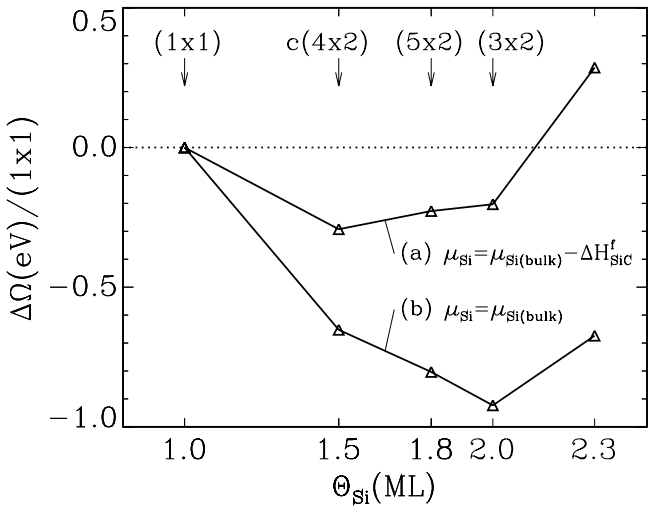

Figure 11. Surface formation energies of our four reconstruction models (triangles) for Si-poor and Si-rich preparation conditions. For Si-poor conditions, the c(4 × 2) model and for Si-rich conditions, the 3 × 2 model has the lowest formation energy. The lines between the triangles are meant as guides to the eye.

hand, the c(4 × 2) reconstruction turns out to be the most stable. Obviously, a surface coverage of $\Theta_{Si} = 2+1/3$ leads to a strong increase of the grand canonical potential and a concomitantly strong decrease of the surface formation energy $\Delta\Omega$ in both cases. The formation energy of the 3 × 2 reconstruction yields the stable minimum in the Si-rich case in agreement with all experimental growth results.

5.2.1. SiC(001)-(2 × 1). The 2 × 1 reconstruction of the SiC(001) surface has been observed in LEED, AES and EELS (see [4, 10]). The experimental data have been interpreted assuming that the observed reconstruction occurs at the clean surface. A reconstruction model with rows of buckled Si dimers with a dimer-bond length of 2.31 Å, very similar to the reconstruction of Si(001)-(2 × 1) [85], was suggested [104]. This interpretation, however, contradicts the results of convergent *ab initio* calculations which find that no strongly bound Si dimers are formed at this surface [12, 24, 28, 105]. The calculations have clearly revealed that the most stable 2 × 1 reconstruction of the clean surface shows only very weakly bound unbuckled dimers. When one considers a reconstruction with fully buckled dimers, as at the Si(001)-(2 × 1) surface [85], the total energy is *raised* by 0.67 eV per unit cell and the surface becomes metallic in contrast to experiment (see [12]). The increase in energy is related to the strong Coulomb repulsion of the bridge bonds with the back bonds due to the small SiC lattice constant, as compared to Si. As a consequence, the fully buckled dimer reconstruction must be discarded at SiC(001)-(2 × 1) and the many previous interpretations of the 2 × 1 and the c(4 × 2) reconstructions in analogy to the buckled dimers at the Si(001) surface do not obtain, therefore. A side view of the optimized atomic structure [12] is shown in the upper left panel of figure 12. Obviously, the 2 × 1 reconstruction of the Si face of SiC(001) is largely different from that of the Si(001)-(2 × 1) surface (see lower left panel of figure 12 for comparison). This is related to the charge transfer from Si to C in SiC and, in particular, to the smaller lattice constant of SiC, as compared to Si. As a consequence, dimer formation at the Si-terminated SiC surface involves much larger back-bond repulsions than at the Si surface. In the optimized structure, the Si surface-layer atoms have moved slightly closer towards each other with respect

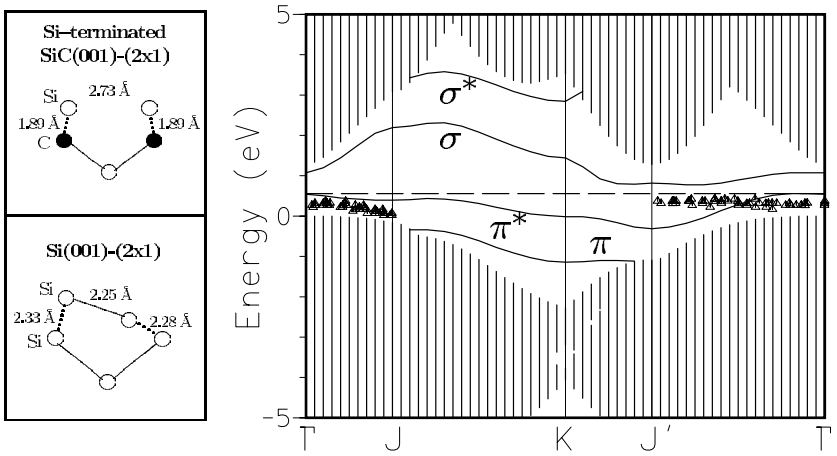

Figure 12. Left panels: side views of the surface atomic structure of the clean Si-terminated SiC(001)-(2 × 1) (top panel) and the Si(001)-(2 × 1) (bottom panel) surface. Right panel: section of the surface band structure of SiC(001)-(2 × 1) (from [12]). The experimental data (triangles) are from [82].

Table 2. Optimized structure parameters (Si–Si bond length d_1 and Si–C bond length d_2, see figure 12) for the 2 × 1 model of the Si-terminated SiC(001) surface from *ab initio* calculations and from experiment [104].

	[12]	[24]	[26]	[28]	[105]	[104]
d_1 (Å)	2.73	2.75	2.26	2.58	2.63	2.31
d_2 (Å)	1.89				1.87	1.91

to their distance at the ideal surface (3.08 Å) and form very weakly bonded Si surface dimers with a bond length of about 2.73 Å [12]. The reconstruction-induced energy gain at this Si face is only of the order of 0.01 eV (10 meV [12], a few millielectronvolt [28]) per dimer, which is much smaller than the energy gain per dimer of about 5 eV at the c(2 × 2) C face. Thus the total energy hypersurface is extremely flat as Si atoms move in the plane of the Si face from a distance of 3.08 to 2.73 Å. If they move further towards each other, the total energy rises. This feature has been reported in excellent mutual agreement from *ab initio* supercell calculations [12, 24, 28, 105]. The most important structure parameters, the dimer-bond length d_1 and the C–Si back-bond length d_2, as resulting from *ab initio* calculations and from experiment are summarized in table 2. The results of Yan *et al* [26] have been obtained with Γ-point sampling only.

A section of the LDA surface band structure of the 2 × 1 surface is shown in the right panel of figure 12. The optimized reconstruction geometry gives rise to a small energy gap and thus to a semiconducting surface. There are four salient surface-state bands in the gap-energy region which originate from the dangling- and bridge-bond bands present at the ideal SiC(001) surface before reconstruction (see [12]). The reconstruction-induced shifts and splittings of the former bands, as well as the nature and origin of the resulting π, $\pi^\star$, σ and $\sigma^\star$ surface-state bands at the reconstructed surface, have been discussed in detail previously [12]. Early angle-integrated PES data clearly show the existence of two occupied surface-state bands in the gap energy region [4, 106]. One of them occurs above the bulk valence band maximum while the other is observed roughly 1 eV below the former. The calculated π and $\pi^\star$ bands in figure 12

can account for these observations. The absolute energy positions and the energetic separation of the two bands by 1 eV, in particular, are well in accord with the data. Furthermore, the band structure of the weakly dimerized 2×1 surface (figure 12) allows us to rationalize four pronounced features in first- and second-derivative EELS spectra [4, 47], as has been shown previously [7, 8]. More recent ARPES investigations of the 2×1 surface have confirmed the existence of two surface-state bands in the above mentioned energy region [79, 82, 100]. In these studies, the dispersion of the surface-state bands has only been measured along the Γ–J and Γ–J′ high symmetry lines in the 2×1 SBZ. The data points from [82] which are in agreement with the results of [79, 100] are included for comparison in the right panel of figure 12. While the calculations show a $\pi^\star$ band of bound surface states with weak dispersion along the Γ–J line and strong dispersion along the Γ–J′ line [12, 79, 107], in experiment [82, 100] only very flat bands are found in this energy region. It appears that there is currently no way to reconcile the calculated π and $\pi^\star$ bands with the measured dispersions of the surface band(s). Fully buckling this surface, in contradiction to the energy minimum requirement, would lead to an even larger dispersion of the respective bands. Also other structural models considered so far [108] do not resolve the puzzle. Further work is necessary to clarify this discrepancy between theory and experiment. We come briefly back to this point in the next subsection.

5.2.2. SiC(001)-c(4×2). Since the early LEED, AES and EELS work of Kaplan [47] and Dayan [67], there has been an ongoing discussion on the structure of the $c(4 \times 2)$ reconstruction of SiC(001) (see [4]). As pointed out above this is related to the fact that it has been a considerable problem to prepare good quality $c(4 \times 2)$ samples for quite some time. Although that obstacle appears to have been overcome more recently, as noted above, the discussion on the structure of the $c(4 \times 2)$ surface remains to be very intensive and has not yet come to a conclusive end [9, 10, 80, 84, 101, 105, 108–114]. The early interpretations of experimental results on the $c(4 \times 2)$ reconstruction in terms of an anticorrelated arrangement of left- and right-tilted asymmetric dimers, analogous to the case of the Si(001)-$c(4 \times 2)$ surface, do not apply since there are no strongly bound asymmetric dimers at the clean Si face of SiC(001) to begin with, as was shown by *ab initio* calculations (see section 5.2.1). Later, experiment has also come to the convincing conclusion that the $c(4 \times 2)$ reconstructions of SiC(001) and Si(001) are largely different (see [10, 80, 115]).

We start our discussion with the *stoichiometric* surface, i.e. with a clean $c(4 \times 2)$ surface terminated by a single Si atom layer. Soukiassian and co-workers, who have made a number of milestone contributions to the field (see [10, 115]), were the first to directly observe the $c(4 \times 2)$ reconstruction using STM. The authors investigated the $c(4 \times 2)$ reconstruction by STM, STS, ARPES and CLS [80, 101, 110, 111]. Based on their STM results, they suggested an entirely new reconstruction model which is largely different from all previously considered reconstructions. Their original model consists of rows of alternatively up and down dimers (AUDD) in the Si surface layer [80]. The dimers were postulated to be symmetric and their bond-length was assumed to be 2.73 Å, a dimer-bond length that had previously been calculated for the clean 2×1 surface [12]. From an analysis of measured filled state STM images and height profiles employing calculated height profiles, as obtained within STM elastic-scattering quantum chemistry simulations based on the extended Hückel approximation, the authors arrived at a reconstruction geometry in which the up-dimers were assumed to remain in the Si surface plane and the down-dimers were relaxed towards the subsurface by 0.1 Å. The AUDD model has one single Si atom layer on the surface in agreement with previous LEED and AES investigations (see [4]). Using this model, excellent agreement between measured and calculated filled state STM images and height profiles was found [80]. The filled state STM

image shows white circular spots, interpreted as being due to the up-dimers, and grey necks located between the circular spots along the dimer rows, interpreted as resulting from the down dimers (0.1 Å below the up dimers). Later on, empty state STM images and height profiles were also interpreted successfully by the group in terms of the AUDD model [111]. In addition, the group has discovered the reversible phase transition, already mentioned above, at about 400 °C between the c(4 × 2) and a 2 × 1 structure [101]. The room-temperature c(4 × 2) surface is found to be semiconducting with a gap of about 1.7 eV while the high-temperature 2 × 1 surface is found to be metallic. Duda *et al* [84] have observed also a phase transition between the c(4 × 2) and a 2 × 1 reconstruction. In their results, both phases were identified as semiconducting, however. The AUDD model has the very charming property of allowing for a simple explanation of the structural phase transition. It is easy to envisage that the up and down dimers all approach the same height with increasing temperature. In that case, a well-ordered 2 × 1 reconstruction should easily form. But that has not been observed in a number of investigations [70, 77, 80, 83, 102]. Instead, the 2 × 1 surface appears to be not well-ordered and has been described as a defective c(4 × 2)* surface with incomplete Si coverage [77], as a surface with defects or impurities [83, 102] or as a 'failed' c(4 × 2) structure [80]. The c(4 × 2) ↔ 2 × 1 phase transition has been described by Hara *et al* [70] as an order–disorder transition. These findings cannot easily be reconciled with the expected behaviour of the simple transition from the c(4 × 2) AUDD to a well-ordered 2 × 1 reconstruction. Finally, it is not easy to understand why such a minor structural rearrangement should give rise to the dramatic change in the surface electronic structure from a gap of 1.7 eV for the c(4 × 2) to basically no gap for the 2 × 1 surface, as observed by Aristov *et al* [101].

Soukiassian and co-workers [110] have also investigated Si 2p surface core-level shifts at the c(4 × 2) surface. They observe spectra with three significant spectral features which are analysed in terms of a five Gaussian least-squares fit. Two of them (S_1 and S_2) are attributed to the up- and down-dimers at the surface, respectively. Two further (SB_1 and SB_2) are interpreted as originating from stress-induced changes in the subsurface and the fifth (B) is shown to be the bulk core level. The core-level shifts of S_1, S_2, SB_1 and SB_2 are determined to be −1.43, −0.54, −0.4 and +0.31 eV, respectively. The first two of these values are in very good accord with the two core-level shifts S_1 and S_2 of −1.4 and −0.5 eV observed earlier by Shek [77] at the c(4 × 2)* surface.

To rationalize their model, Soukiassian and co-workers invoke the relatively small Si–Si distance at the SiC(001) surface as the driving force for this reconstruction. The authors argue that, due to the very large lattice mismatch between the Si and SiC lattice parameters, Si atoms are 'compressed' by some 20% on a Si-terminated SiC(001) surface so that SiC(001) can be viewed as a prototypical case for surface stress effects. Actually, the alternating up and down dimers within the rows are then expected to reduce the surface stress. Certainly, the mismatch between a SiC thin film and the Si substrate on which it is grown gives rise to stress in the SiC samples. It appears, however, not totally clear how much of this stress induced at the interface between Si(001) and SiC(001) remains in effect at the SiC(001) surface a few micrometres, i.e. some 10 000 atomic layers away from the interface even if the stress field decays only as z^{-3}. In any case, the notion of 'compressed' Si atoms *at the surface* seems unjustified. They are neither compressed in bulk SiC nor at the bulk-truncated SiC(001) surfaces since the Si–C bond length in both cases is even larger (due to the ionicity) than the sum of the covalent radii of Si and C and the Si dangling bonds at the surface are free to extend into vacuum. Only when Si atoms move closer together within the Si surface layer upon reconstruction do the relatively large spatial extent of the Si orbitals and the respective increased Coulomb repulsion with the back bonds come into play avoiding strong dimer formation at the 2 × 1 surface, as discussed in section 5.2.1.

Table 3. Structure parameters (as defined in figure 13) for the c(4 × 2) AUDD and c(4 × 2) MRAD models of the Si-terminated SiC(001) surface, as postulated on the basis of STM data [80] and as resulting from *ab initio* structure optimizations by minimizing the total (formation) energy [105, 108, 109, 112, 114]. Results obtained for surfaces under tensile stress are labelled as AUDD⋆.

	Reference	d_{up} (Å)	d_{down} (Å)	Δz (Å)	d_1 (Å)	d_2 (Å)	d_3 (Å)	Δz (Å)
AUDD	[80]	2.73	2.73	0.10				
AUDD	[109]	2.50	2.27	0.23				
AUDD	[112]	2.67	2.40	0.21				
AUDD⋆	[105]	2.62	2.54	0.04				
AUDD⋆	[114]	2.66	2.60	0.04				
MRAD	[108]				2.30	2.35	2.42	0.54
MRAD	[112]				2.36			0.19

More recently, the AUDD model for the c(4 × 2) surface has been studied, as well, by a number of *ab initio* calculations [105, 108, 109, 112–114] which are all based on two-dimensionally periodic supercell geometries, except for the cluster calculation of Douillard *et al* [109]. The calculations of Catellani *et al* [105] have shown that in the total energy minimization process a number of initially assumed c(4 × 2) configurations relax back into the very weakly dimerized 2 × 1 reconstruction, described in the preceding subsection. Lu *et al* [108] have calculated the total energy for the AUDD model proposed in [80] and find it to be higher in energy than the optimized 2 × 1 reconstruction and the ideal 1 × 1 surface. When they allow the atoms in the AUDD model to move freely, the structure is found to move back into the 2 × 1 reconstruction showing that the AUDD model of [80] is unstable. The supercell calculation of Shevlin and Fisher [112] find the AUDD model to be metastable but again it results in higher energy than the ideal 1 × 1 surface. Also the periodic pseudopotential plane wave calculations of Soukiassian *et al* [113] show that the AUDD is not formed without external stress. Only in the cluster calculation of Douillard *et al* [109] is spontaneous AUDD formation observed without external stress.

One of the arguments for suggesting the AUDD in [80] was the expected reduction of surface stress in the model. To this end, Catellani *et al* [105] have investigated the effects of surface stress on the resulting surface geometry by additional supercell calculations. Starting with a 2 × 1 geometry under uniaxial compressive stress, the symmetry of the surface is found to remain unchanged and the dimer bond length increased to 2.75 Å. Only when tensile surface stress is applied, is a very weak c(4 × 2) reconstruction obtained from total energy minimization. This result was confirmed later using supercell calculations by Lu *et al* [114]. The structure of the AUDD reconstruction is schematically shown in the left side of figure 13 and the structural parameters resulting from the different calculations are summarized in table 3. It is to be noted that the different calculations [105, 109, 112, 114] yield qualitatively similar AUDD reconstructions with significant quantitative differences, however. From all total energy calculations an extremely flat energy hypersurface between the ideal 1 × 1, the 2 × 1 and the c(4 × 2) AUDD reconstruction is found [12, 28, 105, 108, 109, 112–114]. This flatness appears to be consistent with the c(4 × 2) ↔ 2 × 1 phase transition, observed at 400 °C by Aristov *et al* [101].

The phase transition has theoretically been addressed, as well, by FP-MD simulations [105]. The extremely demanding computational effort of FP-MD calculations, however, did not allow the authors of [105] to investigate the behaviour of the c(4 × 2) reconstruction as a function of temperature. Instead, Catellani *et al* performed MD simulations of the 2 × 1 reconstruction at 400 and 900 K, thereby keeping the calculations

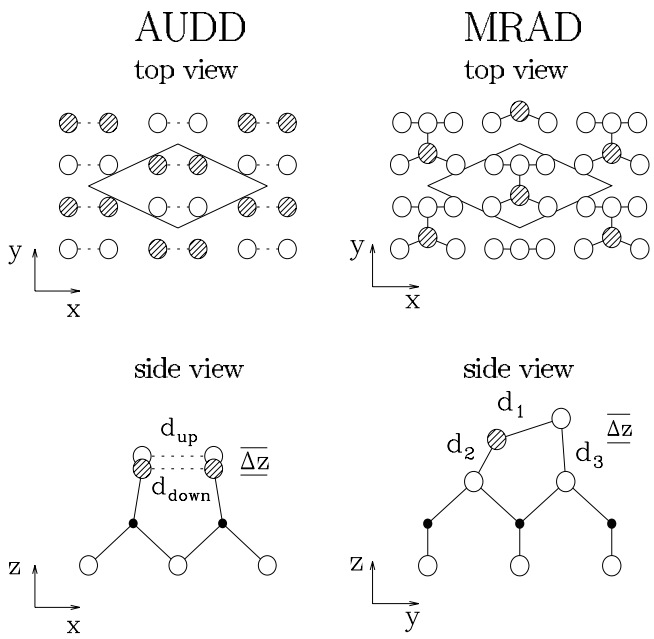

Figure 13. Top and side views of the c(4 × 2) AUDD and the energy-optimized c(4 × 2) MRAD model of the Si-terminated SiC(001) surface. Open or shaded circles represent Si atoms while full dots show C atoms.

manageable and yet allowing them to make contact with experiment. Heating the 2 × 1 surface is found to give rise to large fluctuations of the dimer bond lengths varying between 2.4 and 3.0 Å at 400 K or 2.2 and 3.0 Å at 900 K. Due to the above mentioned flatness of the energy hypersurface disordered configurations were found to occur in the simulation runs. Averaging over quite a number of geometrical configurations when calculating the electronic DOS, Catellani *et al* find that the system on average has a gap of 0.25 eV at 400 K while the gap is almost closed at 900 K. In the latter case the DOS at the Fermi level is very small, however. The authors infer from their results that the 2 × 1 surface is semiconducting at least up to 400 K and shows a tendency to become disordered and weakly metallic well above 400 K. The authors interpret their results for the 2 × 1 surface as an indication that the c(4 × 2) reconstruction might become disordered above 400 K, as well. To which extent these results from FP-MD simulations for 2 × 1 configurations can be viewed as proving evidence for the observed phase transition from a semiconducting c(4 × 2) to a metallic 2 × 1 reconstruction remains a somewhat open question in our opinion.

Catellani *et al* [105] have also calculated STM images for both the 2 × 1 and the c(4 × 2) AUDD reconstruction. The authors find that the two reconstructions give rise to similar STM images for positive voltage and significantly different STM images for negative voltage. Although the comparison between the computed and measured STM images allows for a qualitative interpretation of the data from [80], a quantitative comparison with experiment turns out to be anything but straightforward. Possible effects of the tip electric field as the cause for the observed quantitative differences between theory and experiment are briefly addressed in [105].

Also surface core-level shifts at the clean, well-ordered c(4 × 2) AUDD and the 2 × 1 surface have been investigated by *ab initio* calculations [116]. For the 2 × 1 reconstruction

a variety of defects at the surface, such as missing dimers, adatoms or addimers, has been considered, in addition. Most noticeably, Catellani *et al* do not find any significant difference (within an uncertainty of 0.1 eV) between core-level shifts originating from up and down dimers of the c(4 × 2) AUDD model, a result which is at variance with the interpretation of the experimental CLS data [77, 110]. Also, the authors find neither two nor four core-level shifts but only one of 0.7, 0.9 or 1.0–1.1 eV at the ideal 1 × 1, 2 × 1 and c(4 × 2) surface, respectively. This result can neither account for the two core-level shifts observed by Shek [77] nor for the four core-level shifts observed by Aristov *et al* [110]. Catellani *et al* [116], therefore, argue that the single core-level shift resulting from their calculations for well-ordered surfaces corresponds to the dominant experimental shift (S_1) while the weaker experimental shift (S_2) may originate from an addimer-induced core-level shift. While that discussion of core-level shifts induced by various kinds of defects at the 2 × 1 surface is very revealing, it can nevertheless not resolve the above noted discrepancies for the c(4 × 2) surface since both Shek [77], as well as Aristov *et al* [110], claim to have observed their core-level shifts in well-ordered and well-defined c(4 × 2) reconstructions. As a side remark, we note at this point that an accurate calculation of core-level shifts is a very demanding task, anyway (see [117–119]).

Let us now turn to *nonstoichiometric* models for the c(4 × 2) reconstruction. As noted above, Shek [77] has observed two Si 2p core-level shifts S_1 and S_2 of about −0.5 and −1.4 eV using LEED and soft x-ray photoemission. Based on this finding, the author suggested that the c(4 × 2) surface is terminated by two Si layers rather than by only one. In addition, the theoretical results of Catellani *et al* [105] indicate that the electronic structure of both the clean 2 × 1 and the clean c(4 × 2) AUDD reconstruction is very similar, giving no convincing indication for the largely different energy gaps of the two reconstructions observed in experiment [101]. To address these issues, Lu *et al* [108] have investigated various nonstoichiometric structural models of the c(4 × 2) Si face covered by a full or by partial Si adlayers using *ab initio* total energy and grand canonical potential calculations. A full Si monolayer, as well as half a Si monolayer in three different configurations on top of the Si face, corresponding to a total Si coverage of $\Theta_{\mathrm{Si}} = 2$ or 1.5, respectively, have been investigated. The resulting formation energies as a function of the Si chemical potential μ_{Si} are shown in figure 14. For further comparison, the total energy of the stoichiometric 2 × 1 and c(4 × 2) AUDD surfaces are included as well in the figure. Obviously, the c(4 × 2) missing-row asymmetric-dimer (MRAD) model has by far the lowest formation energy of all c(4 × 2) reconstructions considered. It is lower in formation energy than the AUDD model for all allowed μ_{Si} values. This large energy difference is easily intelligible, since the AUDD model has four unsaturated dangling bonds per unit cell while all these dangling bonds are saturated by addimers in the MRAD model. In the latter, the addimers have only one empty dangling bond per c(4 × 2) unit cell at the dimer down-atom while the dangling bond at the dimer up-atom is fully occupied and chemically inert. The respective occupied surface state band shifts down in energy with respect to symmetric dimers and thereby lowers the total energy considerably. A top and a side view of the MRAD model are shown on the right-hand side of figure 13. It consists of rows of asymmetric dimers in the Si adlayer with every second dimer row missing. Neighbouring dimers are distributed in a staggered arrangement. The other energetically less favourable models, not shown here for brevity, are discussed in [108]. The calculations clearly reveal that the energy of the surface can drastically be lowered by *dimerization* of neighbouring Si atoms in the adatom rows forming c(4 × 2) or 2 × 2 reconstructions. The former of the two is 55 meV per dimer lower in total energy than the latter. The dimers in the half Si adlayer turn out to be asymmetric with a bond length of 2.30 Å. This dimer-bond length is very close to that at the clean Si(001)-(2 × 1) surface [85]. It should be noted that in this model there is no increased Coulomb repulsion of the dimer bonds with Si–C back bonds, as before, since the

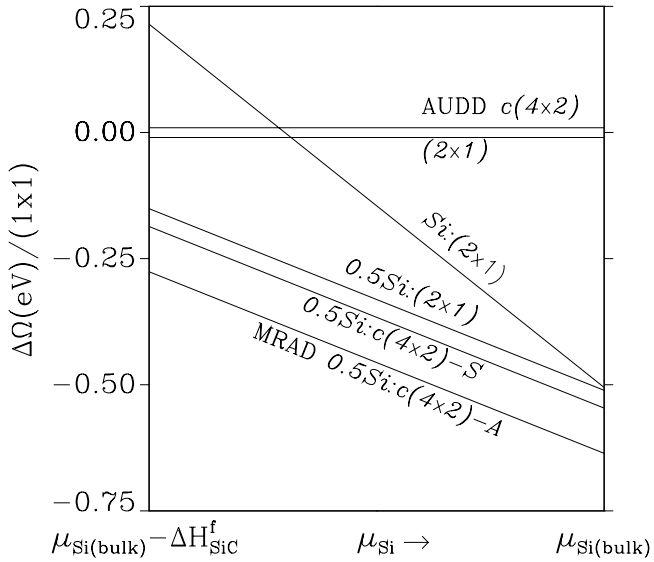

Figure 14. Formation energies for a number of SiC(001) surface models as a function of the Si chemical potential μ_{Si}. A full Si monolayer, as well as three different variants of half a Si monolayer adsorbed on the Si face, are considered. The formation energy of the 2×1 and the c(4×2) AUDD reconstructions are given for further comparison (from [108]).

adatoms reside on a full Si layer at the Si face. In consequence, strong dimers can be formed. The above results are strongly supported by more recent *ab initio* supercell calculations of Shevlin and Fisher [112]. These authors also find the c(4×2) MRAD model to clearly be the most favourable structure for all allowed values of the Si chemical potential even though there are quantitative differences between the results of the two calculations (see table 3). The other calculations mentioned above [105, 109, 113] did not address adatom-induced reconstructions at nonstoichiometric surfaces. If the asymmetric dimers are not distributed in a staggered configuration as in the c(4×2) MRAD model (see figure 13) but are all distributed in parallel and are all buckled in the same direction, an energetically very close 2×2 MRAD structure results [108, 120], as mentioned above. The existence of such 2×2 regions at the surface could explain the occurrence of strong c(4×2) and weak 2×2 LEED spots, as observed by Shek [77] at his so-called c$(4 \times 2)^{\star}$ samples. Finally we note that also in the case of tensile surface stress when the AUDD model becomes weakly stable with respect to the 2×1 reconstruction [105, 114], the MRAD model turns out to be much lower in energy than the AUDD model [114].

The MRAD model can easily explain the occurrence of asymmetric dimers with a short dimer bond length of 2.31 Å, as observed in LEED by Powers *et al* [104]. Furthermore it allows us to rationalize the occurrence of 2×2 LEED spots, as observed by Shek [77]. Since most of the surface preparation procedures, briefly summarized above, arrive at a c(4×2) reconstruction by annealing a Si-rich 3×2 surface, it is very well conceivable that the c(4×2) surface is not terminated by a single Si plane but by 1.5 Si monolayers. At least the calculations of the minimal formation energy clearly show this to be the case. The explanation of the c$(4 \times 2) \leftrightarrow 2 \times 1$ phase transition appears more complicated if one considers the transition from the c(4×2) MRAD reconstruction to the 2×1 reconstruction of the clean Si face, as discussed in section 5.2.1. In order to arrive from the c(4×2) at the clean 2×1 surface,

four Si–Si bonds per unit cell in the MRAD model (the two bonds d_2 and the two bonds d_3 in figure 13) would have to be broken. Although this is not impossible, it would probably take a very high annealing temperature and a long annealing time to achieve it so that it cannot be expected to happen at 400 °C. We have discussed in section 5.2.1 that the single Si layer 2×1 reconstruction yields a surface electronic structure which is at variance with ARPES data. Thus the actual 2×1 reconstruction of the SiC(001) surface is probably different from the one discussed above. In [108] also a structure of half a Si adlayer on top of the Si face with the adatoms in ideal lattice positions of every second row has been considered (0.5Si:SiC(001)-(2×1) or 0.5Si(2×1), for short). This is a competing 2×1 reconstruction whose formation energy is considerably lower for all allowed values of the Si chemical potential than that of the single layer 2×1 surface (see figure 14). Its surface band structure shows only a very small gap while the MRAD model has an LDA gap of 1.1 eV. In this picture, there would be a transition from a clearly semiconducting c(4×2) to an almost metallic 2×1 reconstruction. A phase transition from the c(4×2) MRAD reconstruction to the 0.5Si(2×1) reconstruction would only necessitate breaking one single Si–Si dimer bond per unit cell. While the energy required to break the respective asymmetric dimer bond at the Si(001)-(2×1) surface is 1.6 eV, it amounts to 0.5 eV, only in the case of the SiC(001)-c(4×2) surface [114]. Breaking of this single bond per unit cell at temperatures near 400 °C is easily conceivable, therefore, so that the phase transition including its peculiar semiconductor–metal transition might be explicable that way. Certainly, this phase transition breaking one weak Si–Si surface dimer bond at the c(4×2) surface near 400 °C is much more likely to happen than the thermal desorption of half a Si adlayer necessitating to break four Si–Si bonds per unit cell. The large difference in the gap energies of the c(4×2) MRAD and the 0.5Si:SiC(001)-(2×1) reconstruction would be in very good accord with the data [101]. It needs to be noted, however, at this point that the electronic structure of the latter surface (not shown for brevity) does not resolve the differences between the calculated surface band structure and the ARPES data identified in section 5.2.1 for the 2×1 surface.

The top and side views of the MRAD model in figure 13 reveal that there are six Si atoms per unit cell in the first two layers of the surface. They reside in four different chemical environments, as compared to Si substrate atoms. Thus one can expect that this structure gives rise to four distinctly different surface core-level shifts, as observed in experiment [110]. Two of them, related to the Si up- and down-atoms of the dimers, ought to show different but most pronounced core-level shifts. The Si dimer up- and down-atoms have three Si nearest neighbours each, but reside at different heights above the Si surface plane. The other four Si atoms (two by two of which are equivalent) per unit cell at the second layer (the first complete Si layer), whose chemical environment is also different from that of substrate Si atoms ought to give rise to two additional shifts which might be less pronounced in energy but possibly stronger in intensity. These Si atoms have two C and two Si nearest neighbours instead of four C nearest neighbours as in bulk SiC. They are different since the two atoms on the left have the dimer down-atom as their neighbour in the surface plane while the other two have the dimer up-atom as their neighbour in the surface plane. Concomitantly, the bond lengths d_2 and d_3 are different (see table 3). At this point we can only assume on the basis of the given arguments that the MRAD model might very well give rise to four different core-level shifts. They were not reported in [108], however.

The calculated filled state STM image for the MRAD model is shown in figure 15 in comparison with the measured STM image [80]. Good agreement between theory and experiment should be noted and was found, as well, for respective height profiles [108]. In spite of this good agreement, however, there is an ongoing controversy related to that comparison. While Soukiassian *et al* [80] interpret the spots in their STM image as originating

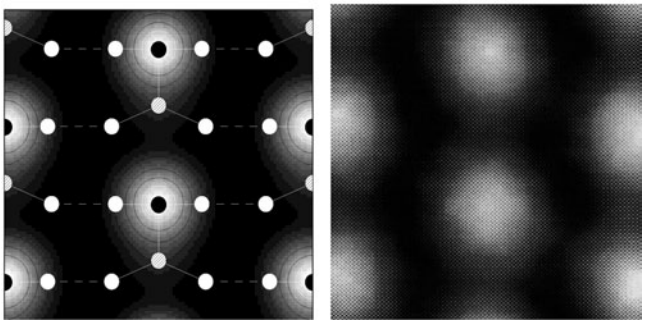

Figure 15. Filled-state STM images of the SiC(001)-c(4 × 2) surface, as measured (right panel) and calculated (left panel) for the MRAD model (from [80, 108]).

from the up-dimers in the AUDD model, Lu *et al* [108] find them in their calculated image to originate from the dimer up-atoms in the MRAD model (see left panel of figure 15). Of course, both interpretations lead to the same pseudohexagonal structure with the same values for the distances between spots. The empty state STM images and height profiles reported later in [111] were also interpreted successfully in terms of the AUDD model and the authors claim that they cannot be reconciled with the empty state image for the MRAD model [108].

Finally, we address the surface band structure of the c(4 × 2) AUDD and MRAD models. To date, the former has not yet been reported in the literature. ARPES measurements of the electronic structure of the c(4 × 2) surface have been reported by Duda *et al* [84]. The authors find the c(4 × 2) surface to be clearly semiconducting and they observe three surface state bands closely above and below the valence band maximum (E_{VBM}). The very flat uppermost band does not occur throughout the SBZ and might be related to surface defects, therefore. The authors compare their data with the available surface band structure of the MRAD model [108] without taking the localization and symmetry properties of the different bands at or near the surface into account. To be able to compare their data with the AUDD model as well, they make use of the fact that Catellani *et al* [105] and Lu *et al* [108] have shown that the electronic structure of the AUDD model is very similar to that of the 2 × 1 surface, a result which is easily intelligible since the AUDD structure is rather similar to the 2 × 1 structure discussed in section 5.2.1. Therefore, Duda *et al* [84] also compare their data for the c(4 × 2) surface with the electronic structure of the 2 × 1 surface (expected to mimic that of the c(4 × 2) AUDD model) which they infer from [12]. The authors conclude from their comparison that the band structure of the c(4 × 2) MRAD model does not agree satisfactorily with their data and that the comparison with the 2 × 1 band structure (meant to approximate that of the c(4 × 2) AUDD model) is even worse. In figure 16 we show the surface band structure of the MRAD model [108] and that of the AUDD model under tensile stress (only in this case a stable structure is found [114]) which we have recently calculated self-consistently on an equal footing for comparison sake. Tensile stress leads to a larger lattice constant and a smaller reciprocal lattice constant in the respective space or reciprocal space directions, respectively. In addition, the larger lattice constant gives rise to a correspondingly smaller projected gap (see figure 16). Surface states with large amplitude on the surface layer are shown as heavy full lines while those originating from lower lying layers are shown as thin full lines. In general, surface resonances are shown by dotted lines but when they are very pronounced heavy full lines are drawn. In both cases the uppermost state in the ARPES data at Γ has been brought into agreement with the highest occupied surface state at Γ since there is usually a rigid shift between calculated and measured bands, depending on the actual Fermi level of

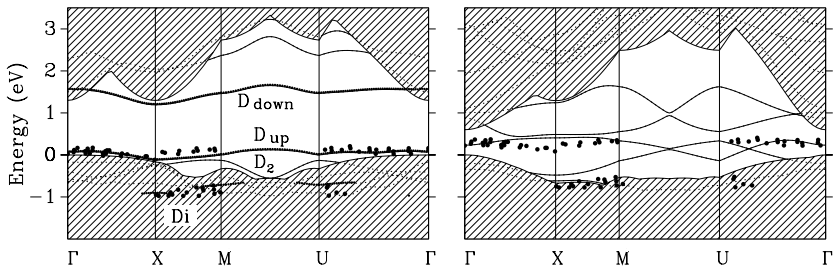

Figure 16. Surface band structure of the MRAD model (left panel, from [108]) and the AUDD model (right panel, this work) of SiC(001)-c(4 × 2) in comparison with ARPES data from [84].

the samples. We note in passing that the surface electronic structure of the 2 × 2 MRAD reconstruction mentioned above has been reported as well [120]. As was to be expected, it largely agrees with that of the c(4 × 2) MRAD model to be discussed in the following. Clearly, the MRAD reconstruction results as semiconducting. The calculated gap of 1.1 eV between the D_{up} and D_{down} bands is somewhat smaller than the experimental gap of 1.7 eV [101] as usual in LDA calculations. Obviously, the calculated D_{up} band originating from the dimer up-atoms in the MRAD model is in excellent agreement with the ARUPS data. Furthermore, the experimental data near −1 eV relative to E_{VBM} are related to the dimer bond band Di. The reason why the band D_2 is not seen in experiment is simply related to the fact that the respective charge density is parallel to the surface plane and is not localized in the surface layer but in the second layer only. This band has been misconstrued in the comparison in [84] as being related to the observed data near −1 eV in the left panel of figure 16. As a consequence, an unsatisfactory agreement between theory and experiment was concluded. The surface band structure of the c(4 × 2) AUDD reconstruction is shown in the right panel of figure 16. First we note that it is very similar to the surface band structure of the 2 × 1 surface backfolded onto the c(4 × 2) SBZ, indeed. Second, it hardly shows any gap. This is at variance with the experimentally observed gap of 1.7 eV [101] even if one accounts for the typical LDA failure to describe semiconductor gaps correctly. Third, the different bands resulting from theory for the AUDD model do not show good systematic agreement with the data. The measured band above E_{VBM} agrees to some extent with the theoretical bands but this apparent agreement seems basically fortuitous in view of the fact that the model supports two bands of different physical origin in this energy region. In particular, between Γ and X, as well as, between U and Γ the theoretical bands fail to describe the measured dispersions appropriately. The backfolding effect alone without any significant structural change seems to be insufficient to produce the experimentally observed dispersion and does not yield the observed large gap of the c(4 × 2) reconstruction at all. Finally, the data points above −1 eV below E_{VBM} are not accounted for by the model. In conclusion, we think that the surface electronic structure of the MRAD model shown in the left panel of figure 16 compares favourably with the ARPES data of Duda *et al* [84]. The agreement between the calculated D_{up} and Di bands and the ARPES data is very satisfactory, lending further support to the MRAD model. The surface band structure for the AUDD model shown in the right panel of figure 16, on the contrary, is not in good agreement with the ARPES data of Duda *et al* [84] and, in particular, with the STS results of Aristov *et al* [101], who determined a gap of 1.7 eV.

In summary, we would like to state that in our opinion the structure of the SiC(001)-c(4 × 2) surface is not unambiguously solved to date. More work seems necessary to address the above identified discrepancies, some of which are related to the AUDD and others to the MRAD model.

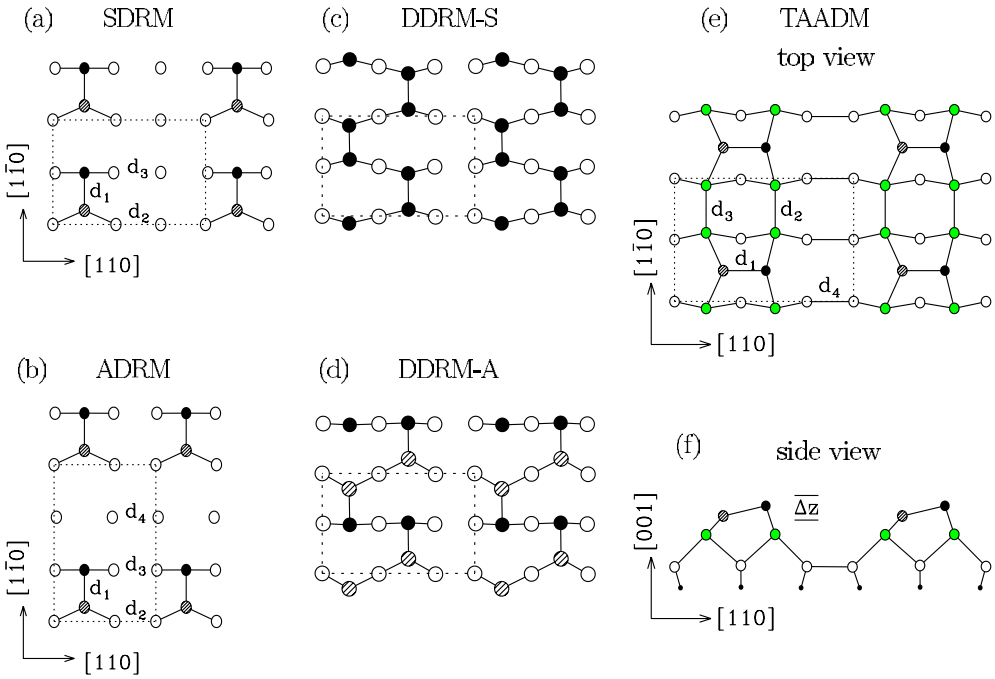

Figure 17. Top views of optimized SDR, ADR, DDR-S, DDR-A and TAAD models of the SiC(001)-(3 × 2) surface (from [121]). A side view of the TAADM is shown in figure 17(f), in addition. The SDRM and ADRM are covered by 1 + 1/3, the DDRM-S and DDRM-A are covered by 1 + 2/3 and the TAADM is covered by 1 + 2/3 + 1/3 monolayers of Si, respectively.

5.2.3. SiC(001)-(3 × 2). As mentioned above, all experimental data agree that the Si-rich 3 × 2-reconstructed surface is covered by an ordered partial Si overlayer on top of the Si face while the actual Si coverage in the adlayer is still a matter of controversial debate. There is conflicting evidence on adatom coverage both from theory, as well as from experiment. Concomitantly, there is considerable controversy concerning the reconstruction of the 3 × 2 surface. Models containing 1/3, 2/3 or 1 Si adlayer on top of the Si face have been proposed and discussed. Their total Si coverage is $\Theta_{\mathrm{Si}} = 1 + 1/3$, $1 + 2/3$ and 2, respectively. Top views of representative structures are shown in figure 17.

In the case of $\Theta_{\mathrm{Si}} = 1 + 1/3$, the adlayer can contain one row of Si adatoms for every three rows of possible bulk spacings along the 3× direction (see figure 17(a)). These Si adatoms can form dimers along the rows, i.e. along the ×2 direction with one addimer per surface unit cell. Such a 3 × 2 single-dimer-row model (SDRM) has been suggested by Hara *et al* [70]. However, it fails to explain STM images measured later by Hara *et al* [75, 76] and by Semond *et al* [78]. Yan *et al* [26] proposed a 2 × 3 alternate-dimer-row model (ADRM) on the basis of *ab initio* calculations. Its unit cell is rotated by 90° with respect to that of the SDRM (see figure 17(b)). In the ADRM the adlayer Si atoms can again form surface dimers but they are now oriented along the ×3 direction. The dimers in both the SDRM and the ADRM have been shown to be strongly asymmetric [121]. Their structure parameters are discussed in [121] in comparison with the results of Yan *et al* [26]. Lu *et al* [121] find the SDRM to be lower in energy by 68 meV per 3 × 2 unit cell, as compared to the ADRM. The ADRM has been used by Semond *et al* [78] to explain STM images and height profiles. Their results appear to support the model in which the asymmetric dimers are oriented and tilted along the ×3

direction. This is, however, in conflict with LEED data [47]. The $\times 3$ direction in the above ADRM is perpendicular to the $2\times$ direction at the 2×1 surface while the LEED pattern for a single domain surface shows it to be parallel to the latter direction. The surface electronic structure of the SDRM has been discussed in detail in [121] in comparison with STM [78, 80] and ARPES [87, 88, 122, 123] data. The SDRM has a semiconducting surface band structure with an LDA gap of about 1 eV. The highest occupied and lowest empty dangling bond bands show only very weak dispersion since the asymmetric dimers are spatially well separated at the surface (see figure 17(a)). Some of the calculated bands show good agreement with experiment but others deviate considerably from the ARPES data. Similar conclusions follow from a comparison of measured and calculated STM images and height profiles [78, 121]. The electronic structure of the ADRM yields even worse agreement with STM and ARPES data. Thus, among the $\Theta_{\mathrm{Si}} = 1 + 1/3$ structures, the ADRM can be excluded on the basis of experimental LEED [47] data and on the basis of *ab initio* total energy calculations [121] which find the ADRM to be less favourable than the SDRM. The SDRM, on the other hand, has not been observed in STM experiments [78] and the dimer direction in the SDRM is in conflict with experimental STM profiles. Based on this experimental and theoretical evidence, we conclude that the Si-rich 3×2 surface is not covered by $1/3$ of a Si monolayer on top of the Si face in any of the above discussed configurations.

For $\Theta_{\mathrm{Si}} = 1 + 2/3$ a number of so-called double-dimer-row models (DDRM) have been investigated. In these models, for every three bulk spacings there are two adatom rows and one missing row. The first DDRM was proposed by Dayan [67] and later adopted by Kaplan [47] and Hara *et al* [75, 76]. Neighbouring Si atoms in the rows can form dimers. Hara *et al* [75] assumed the dimers to be oriented along the rows, i.e. in the $\times 2$ direction. Douillard *et al* [98] have shown, however, that the dimers are oriented along the $3\times$ direction, i.e. perpendicular to the adatom rows. If the dimers are symmetric, two configurations with the two dimers in a row or in a staggered pattern per unit cell can be formed. If the dimers are asymmetric, four different configurations of addimers can be formed (see [121]). To explain their STM data, Hara *et al* [75, 76] considered symmetric dimers of different height above the substrate surface similar to the dimers in the c(4×2) AUDD model [80]. *Ab initio* total energy calculations [121] show, however, that the model is not a stable structure since its total energy is 0.9 eV per unit cell higher than that of the respective asymmetric dimer structures. The calculations show that all four asymmetric dimer DDR reconstructions are much more favourable than those with symmetric dimers [121]. Two representative structures for $\Theta_{\mathrm{Si}} = 1 + 2/3$ are shown in figures 17(c) and (d). The four different DDRMs with asymmetric dimers are very close in total energy within 0.1 eV. They all give rise to a dimer-bond length of about 2.3 Å. The surface electronic structure of the four models is very similar and is not in reasonable agreement with ARPES data [88, 122, 123] and with STM data [75, 76, 78], as was shown in [121]. The same conclusion follows from a comparison of measured [87] and calculated [121] core-level shifts.

In view of the above discrepancies, Lu *et al* [121] have investigated 3×2 structures with larger Si coverage. On the basis of formation energy minimizations they arrived at an optimal structure consisting of two partial adlayers on top of the Si face. The nominal coverage of the surface in this reconstruction is $\Theta_{\mathrm{Si}} = 1+2/3+1/3 = 2$, whereby the Si face (1 monolayer) is covered with a lower adlayer of $2/3$ and an upper adlayer of $1/3$ of a Si monolayer. A top and a side view of this two-adlayer asymmetric-dimer model (TAADM) is shown in figures 17(e) and (f). In this model the lower $2/3$ adlayer has symmetric dimers. The upper $1/3$ Si adlayer on top of the structure features strongly bound asymmetric dimers. These top layer addimers saturate all dangling bonds of the symmetric Si dimers in the second layer. Therefore, there are only two dangling bonds per surface unit cell in the TAADM while there are four dangling bonds per surface unit cell in all DDRM. The bond lengths between Si surface atoms in the

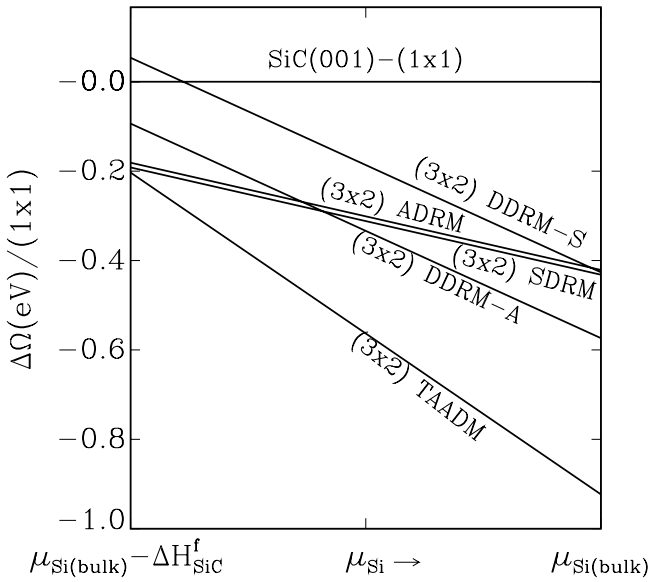

Figure 18. Formation energies of the SDR, ADR, DDR-S, DDR-A and TAAD models of the SiC(001)-(3 × 2) surface as a function of μ_{Si} (from [121]).

TAADM are all close to Si–Si bulk-bond lengths or to the bond length in Si=Si surface dimers, respectively (see [121]). Figure 18 shows the formation energy of the five different structures displayed in figure 17 as a function of the Si chemical potential. It can easily be inferred from the figure that DDRM with symmetric dimers (DDRM-S) are less favourable by roughly 0.15 eV than those with asymmetric dimers (DDRM-A). For C-rich preparation conditions, the ADR and SDR models are more favourable than the DDRM. For all physically allowed values of μ_{Si}, the TAADM is lowest in surface formation energy clearly indicating that the TAADM is the most stable structure of all considered models. This is true, in particular, for the Si-rich case which obtains in experiments when the Si-rich 3 × 2 surface is prepared.

The surface electronic structure of the TAADM, shown in figure 19, compares favourably with ARPES data. It is characterized by salient bands of dangling bond states. A bonding linear combination of dangling bond states at the up- and down-atoms of the dimers in the top layer (see figure 17(f)) gives rise to a band of occupied surface states (D_b) close to the top of the valence bands while an antibonding linear combination of the respective dangling bond states yields an empty band of surface states (D_a) close to the bottom of the conduction bands. Obviously, the TAADM reconstruction is semiconducting. It has an LDA band gap of 0.82 eV. Since the top-layer dimers are well separated in space, the resulting dangling bond bands show only very weak dispersions from Γ to J and M to J′. The dispersion of these two bands in the other $\boldsymbol{k}_{\parallel}$ directions results from sublayer-mediated interactions. The strong chemical bonds in the top-layer asymmetric dimers give rise to a dimer-bond band Di, similar to the one at the Si(001)-(2 × 1) surface [85]. The states giving rise to the bands S_1 and S_2 are localized below the surface plane and are not easy to detect in ARPES or STM measurements, therefore. The surface band structure in figure 19 shows good agreement with ARPES data [88, 122, 123] which are only available for two high symmetry lines of the SBZ. In particular, along Γ–J, the calculated surface-state bands D_b and Di are in good agreement with experiment. Also, along Γ–J′, the D_b band closely follows the measured dispersion.

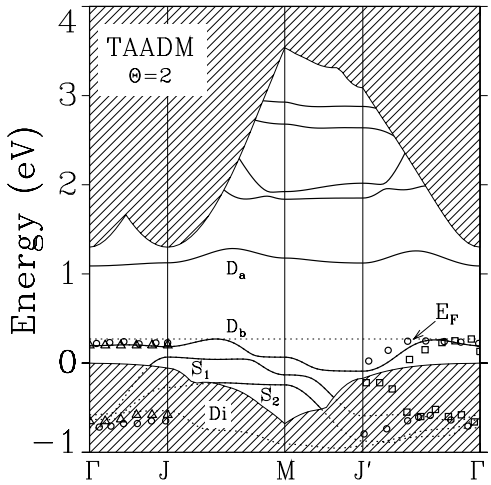

Figure 19. Surface band structure of the TAADM of the SiC(001)-3 × 2 surface. ARPES data from [88, 122, 123] are shown for comparison. To ease the comparison, the uppermost ARPES data point at Γ has been aligned with the highest occupied surface state D_b at the Γ-point by a rigid shift (from [121]).

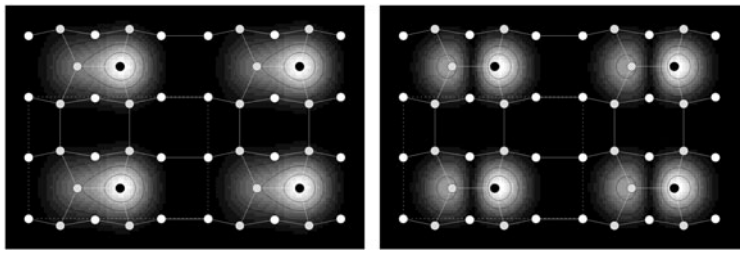

Figure 20. Calculated filled D_b-state and empty D_a state STM images for the TAADM of the SiC(001)-(3 × 2) surface (left and right panel, respectively). The geometry of the surface is superimposed by the top view (see also figure 17(e)) and the rectangular unit cell is indicated by broken lines (from [121]).

Only the relation of the measured band between −0.4 and −0.8 eV in this region of the SBZ to the calculated bands is somewhat more subtle. This might be related to difficulties in experimentally resolving the three calculated bands S_1, S_2 and Di in this energy and $\boldsymbol{k}_\parallel$ region. On the basis of this comparison, we conclude that the calculated surface-state bands in figure 19 are in good agreement with available ARPES data [88, 122, 123]. Benesch *et al* [124] have investigated the 3 × 2 surface very recently by inverse photoemission (ARIPES). They find the 3 × 2 surface to be semiconducting, confirming the above theoretical results. The authors have carefully compared their data with available electronic structure results for the different models addressed above and arrive at the conclusion that the best agreement of their ARIPES data is achieved for the TAAD model. Their lowest measured empty band closely below the bottom of the projected conduction bands shows only very little dispersion and compares favourably with the calculated D_a band in figure 19.

Calculated filled- and empty-state STM images of the TAADM are shown in figure 20. The 3 × 2 reconstruction can clearly be resolved in both images. In the filled-state image, one oval spot per 3 × 2 unit cell can be recognized with the long axis of the spot along the

'3×' direction, i.e. perpendicular to the adatom rows in the lower adlayer. This oval spot splits into two lobes with different intensity in the empty-state image. These characteristic properties of the calculated STM images are in excellent agreement with the experimental findings of Semond *et al* [78]. In the theoretical results [121], the two spots along the '3×' direction are related to the up- and down-atoms of the asymmetric dimers of the top adlayer. The high-intensity spot originates from the dimer up- and the low-intensity spot from the dimer down-atoms. Since the dimer direction in the top adlayer is along the '3×' direction, the height profile observed in STM [78] can be rationalized this way. More detailed discussions on the relation between the ADRM and the TAADM and a number of dimer defects that appear to have been observed in STM experiments [78] may be found in [121]. We note in passing that the calculated core-level shifts for the TAADM [121] are not in satisfactory agreement with the data of Yeom *et al* [87]. Possible reasons for the discrepancies in either experiment or theory or both have been assessed in [121], calling for further studies. In addition, we only briefly note at this point that the ratio of the Si coverage of the 3×2 surface to that of the c(4×2) surface of 1.36, as observed in RHEED by Yoshinobu *et al* [73], is well in accord with the 3×2 TAAD and the c(4×2) MRAD models. We will elucidate this point in more detail at the end of section 5.2.4.

Finally, we briefly address the issue of the behaviour of the surface under H adsorption. Dayan [67] and Hara *et al* [76] have observed a phase transition from the 3×2 to a 3×1 surface by exposing the 3×2 surface to H at room temperature. An opposite phase transition from the 3×1 to the 3×2 surface occurs when the substrate temperature is raised to 1000 °C. This transition has later been observed by other authors [88, 125], as well. But we note at this point that more recent experimental results indicate the persistence of the 3×2 reconstruction after H adsorption [126]. The hydrogen-induced phase transition can occur in two different ways. If the dimers are broken by H termination, each Si atom in a dimer would be terminated by two H atoms saturating its two dangling bonds. In the TAADM, the surface would keep its 3×2 reconstruction since the dimerization is along the '3×' direction. This is not in accord with the experimental observation. A way to reconcile the TAADM with experiment is the abstraction of top layer Si atoms due to H adsorption, i.e. Si surface atoms and H atoms from the gas phase form SiH_4 or Si_2H_6 molecules and desorb from the surface. The phase transition, therefore, can be understood in the following way. First, the Si atoms in the top adlayer of the TAADM are abstracted by exposing the surface to H. The surface then shows a metastable 3×2 DDRM. Second, the hydrogen atoms saturate all dangling bonds of the adatoms in the second adlayer and the weak dimers are broken. The surface then shows a H-induced 3×1 reconstruction. By raising the substrate temperature to 1000 °C, the H atoms desorb and the surface transforms back to a metastable 3×2 DDRM. This way, the amount of Si atoms at the surface would be different before and after the phase transition. The 3×2 DDRM and the 3×2 TAADM may be indistinguishable without careful LEED-IV data. STM measurements before and after hydrogenation would be helpful to analyse whether such a process occurs. On the basis of the above analysis, the STM images should be different before and after hydrogenation.

The TAADM has received further support both from theory and experiment in recent years. Shevlin *et al* [127] have studied a number of 3×2 reconstruction models by *ab initio* total energy and formation energy calculations employing the Car–Parrinello algorithm [34]. Also these authors find the TAADM to be unambiguously favoured for all physically allowed values of the Si chemical potential with respect to the SDR, ADR and DDRM. Calculated bond lengths and the buckling of the top-layer addimers resulting from *ab initio* calculations [121, 127] are in gratifying agreement (see table 4). The remaining differences are certainly related to different k-point sampling used in the calculations. While Shevlin *et al* [127] restrict their SBZ sums

Table 4. Optimized structure parameters in Å (as defined in figure 17(e)) for the TAADM of the Si-terminated SiC(001)-(3 × 2) surface as resulting from *ab initio* calculations in comparison with experimental GIXRD data [131].

	d_1	d_2	d_3	d_4	Δz
[121]	2.24	2.37	2.38	2.41	0.50
[127]	2.31	2.42	2.43	2.41	0.58
[131]	2.42 ± 0.06	2.24 ± 0.05	2.55 ± 0.06	~ 3.08	0.15

to 4 special high-symmetry points (Γ, J, J′, K), Lu *et al* [121] find convergence for 16 general k-points in the SBZ, only. The addimer-bond length was found in [127] to be very sensitive to k-point sampling. A change of about 0.3 Å was observed when going from Γ-point to 4 k-point sampling. This explains why the largest difference in calculated bond lengths in table 4 occurs for d_1. As to the electronic structure, only the bandwidth of the D_b band between ΓJ and ΓJ′ was reported in [127]. The results of [121] (see figure 19) are in somewhat better quantitative agreement with experiment than the numbers given in [127].

We note in passing that Pizzagalli *et al* [128] have also optimized the structure of the SDRM, the ADRM and the DDRM by the Car–Parrinello algorithm (the authors use the labels ADD, ALT and DDR, respectively, for these reconstructions). The authors employ 6×4 surface unit cells and Γ-point sampling corresponding to 4 inequivalent k-points in the 3 × 2 SBZ and find the ADRM to be lowest in formation energy of the three models considered. But the authors did not consider the TAADM in their study which is the most stable 3 × 2 structure, as discussed above. It is interesting to note that filled-state STM images of the ADRM [128] and the TAADM [121] are very similar (see [9]), showing that in both models the topmost adunit is a strongly buckled dimer perpendicular to the Si–Si bonds of the underlying Si layer, i.e. perpendicular to the Si atom rows in the lower adlayer.

A second independent confirmation of the TAADM derives from calculated and measured reflectance anisotropy spectra (RAS). Lu *et al* [129] have calculated RAS from *first principles* for the TAADM, DDRM, SDRM and ADRM and have shown that the energetic positions of the RAS features measured by Rossow *et al* [130] are in excellent agreement with the calculated spectrum for the TAADM. The comparison of the calculated spectra [129] with the RAS data [130] in figure 21 clearly shows that only the spectrum for the TAADM is in good agreement with the data.

The first direct experimental support of the TAADM has been reported only very recently. D'angelo *et al* [131] have used GIXRD as an advanced probe to solve the 3 × 2 structure. The authors use a χ^2 factor analysis to assess the validity of the different models discussed above and find that the TAADM yields by far the most satisfactory value. From the analysis of their GIXRD data they come to the conclusion that the 3 × 2 surface is indeed covered by two partial Si layers above the Si face with the lower one containing 2/3 and the upper one containing 1/3 of a Si monolayer. The qualitative agreement between the novel features of the surface morphology in the TAADM, as suggested by Lu *et al* [121], and the GIXRD data [131] is very rewarding. There are quantitative differences to be noted, however (see table 4). D'angelo *et al* obtain a top-layer addimer bond length which is larger than the theoretical values and alternating long and short Si dimer-bond lengths in the second layer which are much more different than the respective theoretical values. These alternating second layer dimer-bond lengths are thought to be driven by surface stress and to minimize the surface strain which is also considered to be the reason why all addimers in the top layer are tilted in the same direction. The GIXRD measurements rule out the SDR, ADR and DDRM for which no reasonable fitting of the data could be achieved. In contrast, they could favourably be compared with the TAADM

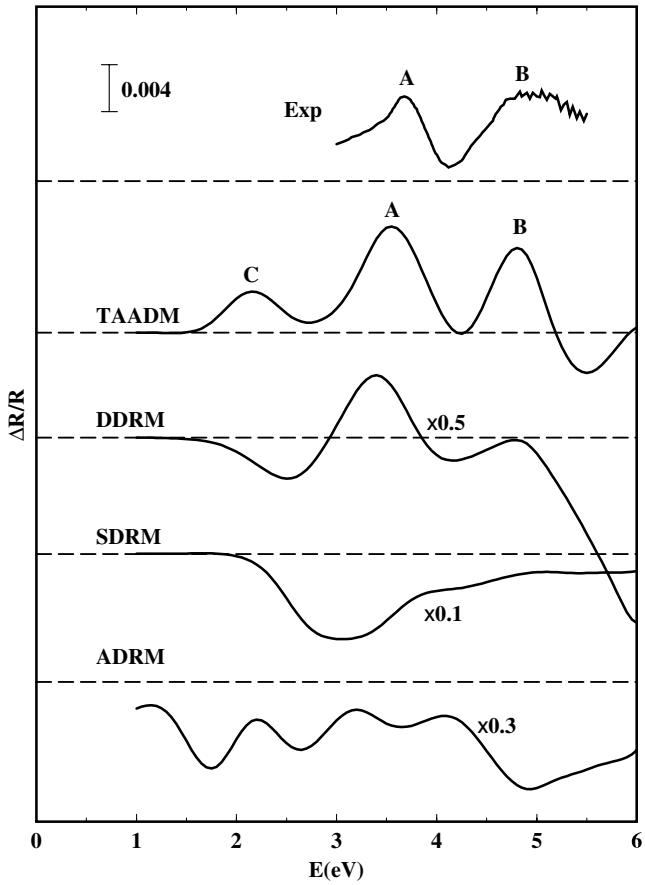

Figure 21. Calculated $\Delta R/R$ spectra (from [129]) for the TAADM, DDRM, ADRM and SDRM in comparison with measured RAS [130].

leading to a successful fitting procedure including the maximum number of parameters. The data clearly support a model of the SiC(001)-(3 × 2) surface reconstruction having three atomic Si planes (1/3 + 2/3 + 1 monolayer from top to bottom) above the first C plane, in agreement with the TAADM [121].

In conclusion, the TAADM with $\Theta_{Si} = 2$ is the most stable 3 × 2 reconstruction among all structures considered so far in the literature. The model is in very good accord with experimental ARPES, STM and RAS data and can account for the coverage ratio as observed in RHEED. In addition, it is in qualitative agreement with the most recent GIXRD data. Only the interpretation of the observed 3 × 2 ↔ 3 × 1 phase transition induced by H adsorption is more subtle calling for Si abstraction by SiH_4 or Si_2H_6 formation, and there are discrepancies between calculated and measured core-level shifts. The DDRM ($\Theta_{Si} = 1 + 2/3$) fail to be in accord with the measured surface band structure and STM images and cannot be reconciled at all with the RHEED data concerning the Si coverage of the surface (for details see section 5.2.4). For $\Theta_{Si} = 1 + 1/3$, the ADRM can be excluded on the basis of LEED data and the SDRM fails to explain the measured STM images, especially the two spots per unit cell along the 3× direction in the empty-state STM image. In addition, the DDR, ADR and SDR models are only metastable and they cannot account for the GIXRD and RAS data.

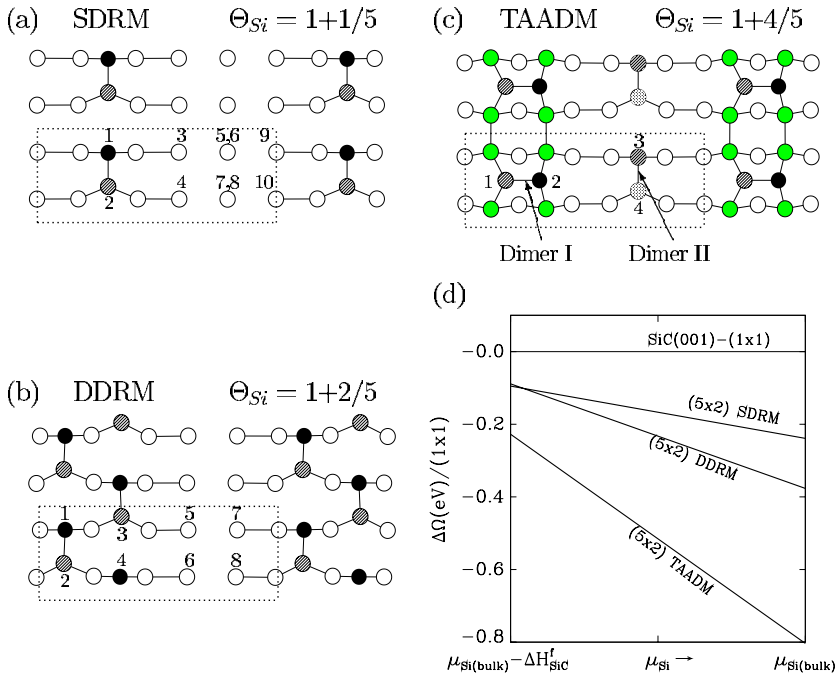

Figure 22. Top views of the optimized 5 × 2 structures for the (a) SDR, (b) DDR and (c) TAAD models. The 5 × 2 unit cells are indicated by broken lines. The open circles represent the substrate–surface Si atoms and the others represent Si adatoms. In the panel of the TAADM, dotted circles represent adatoms in the lower adlayer and solid circles, and the line-shaded circles indicate adatoms in the top adlayer. Both dimer I and dimer II in the top and in the lower adlayer are asymmetric. In each unit cell the unsaturated dangling bonds are indicated by respective numbers. The lower right panel (d) shows the surface formation energy for the three different structures as a function of μ_{Si} (from [132]).

5.2.4. SiC(001)-(5 × 2). In the case of the Si-rich 5 × 2 reconstruction also, all experimental data agree that the surface is covered by an ordered partial Si overlayer on top of the Si face. However, the actual Si coverage in the adlayer is not unequivocally known, to date (see [4, 10]). Several reconstruction models similar in character to the 3 × 2 reconstructions discussed in section 5.2.3 have been suggested in the literature. Among these, SDRM, DDRM and TAADM have been considered [67, 75, 76, 132]. Top views of three representative structures are shown in figure 22. They contain 1/5, 2/5 or 4/5 Si adlayers on top of the Si face so that their total Si coverage is $\Theta_{Si} = 1 + 1/5, 1 + 2/5$ and $1 + 4/5$, respectively. As in the case of the 3 × 2 reconstruction, the ADRM can be excluded on the basis of LEED observations. In the SDRM, the adlayer contains *one* row of Si adatoms for every *five* rows of substrate–surface atoms (see figure 22(a)). The adatoms form asymmetric dimers with a bond length of 2.28 Å, a buckling angle of 13.7° and a tilt height of 0.54 Å [132]. These values are nearly the same as in the SDRM for the 3 × 2 surface (see section 5.2.3) indicating that the correlation between the dimer rows is negligible in both cases. The substrate–surface atoms near the adatom rows move towards each other and form weakly bound symmetric dimers. In addition, there is one row of atoms per unit cell in the Si face which is not involved in dimer bonding, at all. There are ten unsaturated dangling bonds per unit cell in the SDRM which is energetically very unfavourable. In the DDRM, first suggested by Dayan [67] and Hara *et al* [70, 75], the adlayer contains *two* rows of Si adatoms for every *five* rows of

Si substrate–surface layer atoms. The adatoms in the rows form asymmetric dimers in the row direction, as well. A number of different arrangements of the dimers in the two neighbouring rows like at the 3×2 surface is possible, giving rise to slightly different 5×2 DDR reconstructions. The total-energy difference between the respective structures is very small and the electronic properties are very similar [132]. The DDR structure shown in figure 22(b) has the lowest total energy among the considered DDR structures. The dimers in neighbouring rows are arranged in zigzag chains and all dimers are tilted in the same direction. The dimer-bond length in the adlayer is 2.31 Å and the buckling angle is 16°. All atoms in the substrate–surface layer are bonded with adatoms or other surface atoms. Therefore, the total number of unsaturated dangling bonds per 5×2 unit cell in the DDRM is reduced to eight (see figure 22(b)).

As for the 3×2 surface, also for the 5×2 surface a TAADM structure has been suggested [132]. There are again two partial Si adlayers on top of the Si face in this model (see figure 22(c)) but the lower one now contains $3/5$ and the upper one $1/5$ of a Si monolayer. The lower adlayer contains three rows of Si adatoms for every five rows of substrate–surface atoms. Laterally, these three adatom rows are arranged per unit cell in the order of two adatom rows, one missing adatom row, one adatom row and one missing adatom row. The atoms of the upper adlayer adsorb on the two neighbouring adatom rows in the lower adlayer. The total Si coverage of this structure is $\Theta_{\mathrm{Si}} = 1 + 4/5$, therefore. There is one dimer in the top adlayer (dimer I) and one dimer in the lower adlayer (dimer II). Both of these dimers are highly asymmetric and they are oriented in perpendicular directions. Dimer I is formed along the '$5\times$' direction and dimer II is formed along the '$\times 2$' direction. As a consequence, the interaction between these dimers is relatively small. It turns out that dimer I of the 5×2 TAAD reconstruction is very similar to the surface dimer at the 3×2 TAAD model. It has a bond length of 2.25 Å and a buckling angle of 12.9°. Dimer II is very similar to the dimer in the c(4×2) MRAD model with a bond length of 2.28 Å and a buckling angle of 13.3°. Most of the dangling bonds of the Si surface atoms are saturated by adatoms or by dimerization in the 5×2 TAADM. In total, only four unsaturated dangling bonds per 5×2 unit cell exist originating from the up and down atoms of dimers I and II, respectively (see figure 22(c)). Compared with ten dangling bonds in the SDRM and eight in the DDRM, the TAADM with only four dangling bonds turns out to be by far the most stable of these structures. This is most obvious from the formation energies shown for the different models as a function of μ_{Si} in figure 22(d). The DDRM is more stable than the SDRM but throughout the whole range of accessible values of the Si chemical potential, the TAADM has by far the lowest formation energy. These results are consistent with the number of unsaturated dangling bonds at the respective surfaces, as noted above.

The electronic structure of the 5×2 TAADM was reported in [120, 132]. Since there are no ARPES or ARIPES data available for comparison to date, we only briefly comment on the surface band structure and refrain from showing it explicitly, for brevity. The surface is semiconducting with an LDA gap of 0.85 eV. The surface band structure is characterized by two occupied dangling bond bands near E_{VBM} with a rather small dispersion and two empty dangling bond bands near the bottom of the projected conduction bands also with a very small dispersion. Actually, it has been shown in [120] that the structure of the 5×2 TAADM is a simple superposition of the structures of the 2×2 MRAD and the 3×2 TAAD models. Likewise, the electronic structure results as a superposition of that of the 2×2 MRAD and 3×2 TAAD models since dimer I and dimer II in the 5×2 unit cell have only a very small interaction. They point in perpendicular directions and are fairly far apart. Only the long-range order of the dimers at the 5×2 surface is different from that at the 3×2 TAADM and the 2×2 or c(4×2) MRAD models, respectively, but the short-range configuration of the main

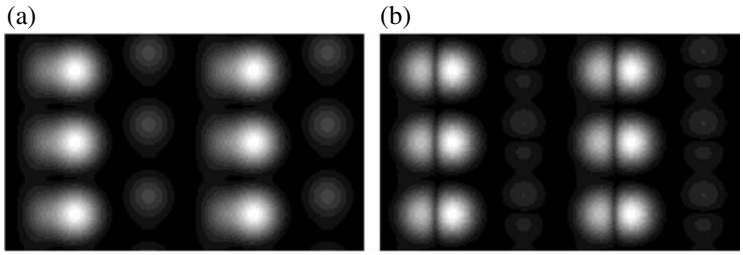

Figure 23. Calculated (a) filled-state and (b) empty-state STM images for the 5×2 TAADM (from [132]).

building blocks (dimer I and dimer II) of the reconstruction are very similar to those at the 3×2 TAAD and the 2×2 or c(4×2) MRAD models, respectively.

The 5×2 reconstruction has been observed in STM by Hara *et al* [75, 76], Kitamura *et al* [81] and by Soukiassian *et al* [133]. Only filled-state STM images and height profiles have been reported. An oval-shaped filled-state image is found. The long axis of the oval spot is along the '$5\times$' direction. It was also found that the 5×2 surface has the same crystallographic basis as the 3×2 surface [133]. Calculated filled- and empty-state STM images for the TAADM are shown in figure 23. In the filled-state image there is one bright oval-shaped spot and one fairly dark round spot in each unit cell. The oval and the round spots originate from dimer I and from the up atom of dimer II, respectively. The oval spot is much brighter than the round one since dimer I is localized at the top adlayer while dimer II is located 1.3 Å lower in the z direction. In the STM experiments [76] only the oval spot has been observed. This could be due to the experimental resolution which might not be high enough to resolve the contribution from the low-lying up-atom of dimer II. In the empty-state STM image the former oval spots split into two spots with different intensity while the former faint round spots split into two spots in the perpendicular direction since dimer II is perpendicular to dimer I in the TAADM. The two bright spots from dimer I are arranged in the '$5\times$' and the two dark spots from dimer II in the '$\times 2$' direction. All features in figure 23 show the asymmetry of dimers I and II. A more detailed comparison of calculated and measured STM images and height profiles may be found in [132]. In conclusion, the calculated filled-state STM image shows a bright oval-shaped spot in each 5×2 unit cell which is consistent with the experimental observations.

Finally, we address once more the question of the Si coverage of the 3×2 and 5×2 surfaces in relation to that of the 2×1 or c(4×2) surfaces. As noted earlier, Hara *et al* [70] have shown that the coverage of the 5×2 surface is lower than that of the 3×2 and higher than that of the c(4×2) surface. In addition, a number of experimental studies have revealed that the 2×1 surface has basically the same Si coverage as the c(4×2) surface (see [4]). Furthermore, Yoshinobu *et al* [73] have investigated transitions from the c(2×2) C face to 3×2, 5×2 or 2×1 Si faces in dependence of the amount of Si_2H_6 dose by RHEED. They found that the dose required for the transition to the Si-rich 3×2 and 5×2 surfaces is approximately 1.36 and 1.16 times as large as the dose necessary for the transition to the c(4×2) or 2×1 surfaces, respectively. To check the consistency of the various models discussed in this section with these observations we have calculated the coverage ratios of all 3×2 or 5×2 and c(4×2) models addressed. Of course, the coverage ratio of a particular pair of models depends sensitively on the coverage of both single models defining the pair. The results are given in table 5.

As is very obvious from the table only the pairs consisting of the AUDD and the SDR models or the MRAD and the TAAD models are in very good agreement with the RHEED

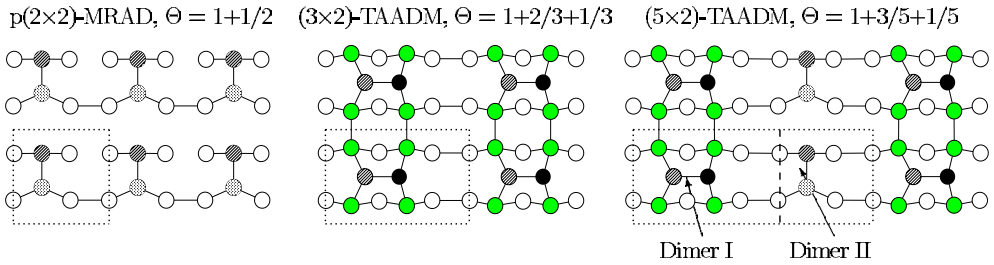

Figure 24. Top views of the optimized surface structure of the 2 × 2 MRAD, the 3 × 2 TAAD and the 5 × 2 TAAD reconstructions of SiC(001). Note that the unit cell of the optimized 5 × 2 surface is a mere superposition of the unit cells of the optimized 3 × 2 and 2 × 2 surfaces (from [120]).

Table 5. Ratios $r_n = \Theta_{n\times2}/\Theta_{c(4\times2)}$ with $n = 3$ and 5 for the 3 × 2 and 5 × 2 SDR, DDR and TAAD models in relation to the c(4 × 2) AUDD and MRAD models of SiC(001). The calculated values should be compared to the measured ratios $r_3 = 1.36$ and $r_5 = 1.16$ from [73].

	Si coverage	AUDD $\Theta_{c(4\times2)} = 1.0$	MRAD $\Theta_{c(4\times2)} = 1.5$
SDRM	$\Theta_{3\times2} = 1.33$	$r_3 = 1.33$	$r_3 = 0.89$
	$\Theta_{5\times2} = 1.20$	$r_5 = 1.20$	$r_5 = 0.80$
DDRM	$\Theta_{3\times2} = 1.67$	$r_3 = 1.67$	$r_3 = 1.11$
	$\Theta_{5\times2} = 1.40$	$r_5 = 1.40$	$r_5 = 0.93$
TAADM	$\Theta_{3\times2} = 2.00$	$r_3 = 2.00$	$r_3 = 1.33$
	$\Theta_{5\times2} = 1.80$	$r_5 = 1.80$	$r_5 = 1.20$

results for the coverage ratios r_3 and r_5. The first pair, however, has to be discarded, since the SDR models are in disagreement with a host of experimental and theoretical results. As a consequence, only the pair consisting of the MRAD and the TAAD models is consistent with the measured coverage ratios *and* all the other experimental and theoretical evidence, as identified above. Obviously, the pair consisting of the AUDD [80] and the 3 × 2 TAAD model [121, 131] leads to strong disagreement ($r_3 = 2.00$ instead of 1.36) with the RHEED results [73]. Likewise, all combinations which include DDRM fail to yield coverage ratios in agreement with these experiments.

5.2.5. SiC(001)-(n × 2). Finally, we briefly address higher $n \times 2$ reconstructions. On the basis of experimental STM results, such reconstructions have been discussed, for example, in detail by Hara *et al* [75], by Kitamura *et al* [81] and by Soukiassian and co-workers [98, 133]. Based on independent calculations, $n \times 2$ reconstructions were suggested to result from superpositions of two basic building blocks. Pollmann *et al* [120] considered superpositions of the 2 × 2 MRAD and the 3 × 2 TAAD reconstructions. Shevlin *et al* [127] addressed in their tight binding calculations $n \times 2$ structures as originating from superpositions of c(4 × 2) MRAD and 3 × 2 TAAD reconstructions. The difference between the suggested reconstructions [120, 127] simply lies in the different distribution (staggered versus parallel) of the asymmetric dimers in the c(4 × 2) or 2 × 2 MRAD units, respectively. This small structural difference, which has not yet been addressed by *ab initio* calculations, can be expected to yield small total energy differences only, and basically the same surface electronic structure for a given $n \times 2$ reconstruction. Figure 24 shows the energy optimized 5 × 2 TAAD model, discussed in section 5.2.4, in direct comparison with the energy optimized 2 × 2 MRAD

and 3×2 TAAD models. The figure clearly reveals that the 5×2 TAAD structure is just a superposition of the 3×2 TAAD and 2×2 MRAD structures. In the 2×2 MRAD model, the asymmetric surface dimer above the Si face is the building block of the reconstruction while in the 3×2 TAADM the Si adatoms on the two partial adlayers above the Si face form a surface hexamer as the building block of the reconstruction. We label these structural units A and B, respectively. Since there is little interaction between the different units, as we have seen for the 5×2 surface, we can generate a number of distinctive reconstructions with a minimum number of dangling bonds per unit cell by cutting and pasting appropriate sections of figure 24 employing the following recipe:

A	2×2	MRAD	
B	3×2	TAADM	
AB	5×2	TAADM	
AAB	7×2	TAADM	
ABB	8×2	TAADM	
AAAB	9×2	TAADM	
AABB	10×2	TAADM	
ABBB	11×2	TAADM	(I)
AAAAB	11×2	TAADM	(II)

Note that all higher $n \times 2$ reconstructions (with $n \geqslant 7$) can be formed but there is no 4×2 or 6×2 reconstruction. Actually, these latter two reconstructions have never been observed in experiment. This observation has previously led to the notion that the Si face of SiC(001) shows only $n \times 2$ reconstructions with n being odd [75]. But Douillard *et al* [98] have more recently observed an even 8×2 reconstruction. The authors found pairs of self-assembled atomic lines in an 8×2 reconstruction being a combination of alternating periodic 3×2 and 5×2 unit cells. A clear 8×2 LEED photograph was seen and a number of patterns with various lines of dimers, stacked perpendicular to the line directions, were observed. The filled-state STM image of the 8×2 surface shows very clearly a periodic arrangement of a pair of lines with dimers perpendicular to the lines and a missing line. The distances d_1, d_2 and d_3 between neighbouring lines in a unit cell, neighbouring unit cells and neighbouring dimers along the lines were found to be 9 ± 1, 25 ± 1 and 5.8 ± 0.9 Å, respectively. In the light of the above considerations, the only possible 8×2 reconstruction is an ABB structure which is a combination of one 2×2 (A) and two 3×2 (BB) structural units. We can view this structure equally well as an AB and a B part, the former of which is a 5×2 and the latter a 3×2 building block. This way, the whole structure becomes a combination of alternating 5×2 and 3×2 units in accord with the experimental observations [98]. If we look, in particular, at the resulting geometry we have one A unit with dimers on the lower adlayer along the $\times 2$ direction giving rise to the missing line in the filled-state image. In addition, we have two neighbouring B units, each of which with a line of dimers on the top layer which are stacked perpendicular to the lines giving rise to the pair of dimer lines in the STM image. The distances mentioned above can be read off from an appropriate extension of figure 24 to the ABB 8×2 structure. In terms of the nearest neighbour distance $d = 3.08$ Å, they are given as $d_1 = 3d = 9.24$ Å, $d_2 = 8d = 24.64$ Å and $d_3 = 2d = 6.16$ Å. This excellent agreement with the measured distances corroborates the general assessments made above. In spite of this nice agreement it should be noted, however, that Doulliard *et al* [98] have interpreted their STM height profiles as showing that the dimers in the lines appear to be symmetric. In the ABB model, however, they are asymmetric as on the 3×2 or 5×2 surface. In our opinion. the filled-state height profiles in [98] do not prove free from doubt that the dimers are symmetric since only distances between maxima in the rows (d_1), minima between the rows (d_2) and distances between neighbouring dimers along a row (d_3) are

determined. Independent of the dimers being symmetric or asymmetric, these distances are $3d$, $8d$ and $2d$, respectively. We note in passing that in [98] an actual structure model for the 8×2 reconstruction was set up with a Si coverage of 1.25, i.e. between that of the 3×2 SDRM (1.33) and the 5×2 SDRM (1.2) to account for the measured coverage ratios (see [73, 75] and table 5). This model is questionable, however, in view of the results for the 3×2 TAAD and 5×2 TAAD reconstructions discussed above. In general, it is easily intelligible on the basis of the above discussion of $n \times 2$ reconstructions that many different patterns of self-assembling parallel dimer lines can occur, as has been observed in experiment [10, 81, 98, 115, 133]. For example, starting from the 11×2 reconstruction, two different configurations (I and II) of the A and B units as indicated above can occur which give rise to 11×2 structures with different arrangements of the top layer dimer lines. Kitamura *et al* [81] have observed various arrangements of such dimer lines and even a 15×2 structure in STM (see figure 1 in [81]) which can be rationalized by the two configurations of A and B units which are possible for $n = 15$. When a given reconstruction consists, in particular, of many A units and only one B unit per unit cell, the result is a structure featuring spatially well-separated single lines of Si dimers (atomic wires) in the top adlayer of the B unit. Many beautiful realizations of such dimer line configurations (see figures 1–3 in [98] and figures 2 and 3 in [133]) have been observed by Soukiassian and co-workers [10, 98, 115, 133].

6. Conclusions

In this paper we have discussed relaxation and reconstruction models of cubic SiC surfaces and their respective electronic structure and STM images. The relaxed nonpolar SiC(110) surface shows a bond-length-contracting rotation–relaxation very much like the surfaces of other ionic wide bandgap semiconductors. The reconstructions of C- or Si-terminated polar (111) and (001) surfaces are very different from the reconstructions of the respective elemental group IV semiconductors diamond and Si. The electronic structure of 3C-SiC(111) surfaces cannot be interpreted within a one-particle picture. Correlation effects need to be taken into account to achieve agreement with ARPES and ARIPES data leading to a Mott–Hubbard picture for the SiC(111) surfaces. The C-terminated SiC(001) surface exhibits triple-bonded C≡C surface dimers in a staggered configuration, the BD model, while Si-terminated SiC(001) surfaces show a rich variety of surface structures spanning the range from a well ordered 2×1 surface to reconstructions which feature even well-separated Si dimer lines (atomic wires) at the surface. All SiC(001) reconstructions are entirely different from those of the C(001)-(2×1) or Si(001)-(2×1) surfaces which is largely due to the small covalent radius of C, to the respective ionicity of SiC and to the large difference in lattice constants between the diamond, Si and SiC bulk crystals. The Si-terminated structures, in general, are very complex. The large Si orbitals in the relatively small surface-layer unit cell of SiC(001) give rise to entirely novel reconstructions which are formed by Si uptake from the gas phase. Employing two basic building blocks, 2×2, c(4×2), 3×2, 5×2 and many higher $n \times 2$ structures with $n \geqslant 7$ can easily be formed. One of these building blocks is a Si dimer, as in the c(4×2) or 2×2 MRAD structure. The other is a Si hexamer as in the 3×2 TAAD structure. The higher reconstructions have different numbers of both building blocks, the Si dimer and the Si hexamer, per unit cell. We have seen that the results of well-converged *ab initio* total and formation energy minimization and electronic structure calculations yield good agreement with experimental data of surface structure determinations and high-resolution surface spectroscopy measurements for a large number of reconstructions. Yet, significant deviations between theory and experiment remain in some cases, most noticeably for some aspects of the reconstructions of Si-terminated SiC(001) surfaces. The good agreement between theoretical results with

many recent experimental data on a number of these surfaces confirms the appropriateness and usefulness of most advanced 'state of the art' theoretical approaches for quantitative studies of well-defined semiconductor surfaces.

We have not only identified the solved but also the open questions to be addressed in the near future at the end of each subsection of the paper. Therefore, we refrain from listing all of these statements once more at this point.

Acknowledgments

We would like to acknowledge Wenchang Lu, Albert Mazur, Michael Rohlfing, Magdalena Sabisch and Fu-He Wang for their contributions to the results discussed in this paper. In addition, we acknowledge financial support of this work by the Deutsche Forschungsgemeinschaft (Bonn, Germany) under contracts no Po 215/13-1,2,3 and grants of Cray computer time at the John von Neumann-Institute for Computing (NIC) of the Forschungszentrum Jülich (Germany) under contract no K2710000.

References

[1] Bechstedt F, Käckell P, Zywietz A, Karch K, Adolph B, Tenelsen K and Furthmüller J 1997 *Phys. Status Solidi* b **202** 5
[2] Choyke W J, Matsunami H and Pensl G (ed) 1997 *Silicon Carbide, A Review of Fundamental Questions and Applications to Current Device Technology* (Berlin: Akademie Verlag)
[3] Bermudez V M 1995 *Appl. Surf. Sci.* **84** 45
[4] Bermudez V M 1997 *Phys. Status Solidi* b **202** 447
[5] Lambrecht W R L, Limpijumnong S, Rashkeev S N and Segall B 1997 *Phys. Status Solidi* b **202** 5
[6] Pollmann J, Krüger P, Rohlfing M, Sabisch M and Vogel D 1996 *Appl. Surf. Sci.* **104/105** 1
[7] Pollmann J, Krüger P and Sabisch M 1997 *Phys. Status Solidi* b **202** 421
[8] Pollmann J and Krüger P 2000 *Handbook of Surface Science* vol 2, ed K Horn and M Scheffler (Amsterdam: Elsevier) p 94
[9] Catellani A and Galli G 2002 *Prog. Surf. Sci.* **69** 101
[10] Soukiassian P 2002 *Mater. Sci. Eng.* B **96** 115
[11] Sabisch M, Krüger P and Pollmann J 1995 *Phys. Rev.* B **51** 13367
[12] Sabisch M, Krüger P, Mazur A, Rohlfing M and Pollmann J 1996 *Phys. Rev.* B **53** 13121
[13] Rohlfing M and Pollmann J 2000 *Phys. Rev. Lett.* **84** 135
[14] Hohenberg P and Kohn W 1964 *Phys. Rev.* B **136** 864
[15] Kohn W and Sham L J 1965 *Phys. Rev.* A **140** 1133
[16] Ceperley D M and Alder B I 1980 *Phys. Rev. Lett.* **45** 566
[17] Perdew J P and Zunger A 1981 *Phys. Rev.* B **23** 5048
[18] Perdew J P and Wang Y 1986 *Phys. Rev.* B **33** 8800
Perdew J P, Burke K and Wang Y 1996 *Phys. Rev.* B **54** 16533
[19] Hamann D R, Schlüter M and Chiang C 1979 *Phys. Rev. Lett.* **43** 1494
Hamann D R, Schlüter M and Chiang C 1984 *Phys. Rev.* B **32** 393
Bachelet G B, Hamann D R and Schlüter M 1982 *Phys. Rev.* B **26** 4199
[20] Vanderbilt D 1990 *Phys. Rev.* B **41** 7892
[21] Troullier N and Martins J L 1991 *Phys. Rev.* B **43** 1993
[22] Kleinman L and Bylander D M 1982 *Phys. Rev. Lett.* **48** 1425
[23] Wenzien B, Käckel P and Bechstedt F 1994 *Surf. Sci.* **307–309** 989
[24] Käckell P, Furthmüller J and Bechstedt F 1996 *Appl. Surf. Sci.* **104/105** 45
Käckell P, Furthmüller J and Bechstedt F 1996 *Surf. Sci.* **352–354** 55
[25] Käckell P, Furthmüller J, Bechstedt F, Kresse G and Hafner J 1996 *Phys. Rev.* B **54** 10304
[26] Yan H, Smith A P and Jónsson H 1995 *Surf. Sci.* **330** 265
[27] Northrup J E and Neugebauer J 1995 *Phys. Rev.* B **52** R17001
[28] Catellani A, Galli G and Gygi F 1996 *Phys. Rev. Lett.* **77** 5090
[29] Sabisch M, Krüger P and Pollmann J 1997 *Phys. Rev.* B **55** 10561
[30] Ihm J, Zunger A and Cohen M L 1979 *J. Phys. C: Solid State Phys.* **12** 4409
[31] Scheffler M, Vigneron J P and Bachelet G 1985 *Phys. Rev.* B **31** 6541
[32] Krüger P and Pollmann J 1991 *Physica* B **172** 155

[33] Broyden C G 1965 *Math. Comput.* **19** 577
See also Johnson D D 1988 *Phys. Rev.* B **38** 12807
[34] Car R and Parrinello M 1985 *Phys. Rev. Lett.* **55** 2471
[35] Payne M C, Teter M P, Allan D C, Aruas T A and Joannopoulos J D 1992 *Rev. Mod. Phys.* **64** 1045
[36] Qian G-X, Martin R M and Chadi D J 1988 *Phys. Rev.* B **38** 7649
[37] Northrup J E and Froyen S 1993 *Phys. Rev. Lett.* **71** 2276
[38] Kubaschewski O and Alcock C B 1979 *Metallurgical Thermochemistry* (Oxford: Pergamon)
[39] Krüger P, Mazur A, Pollmann J and Wolfgarten G 1986 *Phys. Rev. Lett.* **57** 1468
[40] Krüger P and Pollmann J 1988 *Phys. Rev.* B **38** 10578
[41] Tersoff J and Hamann D 1985 *Phys. Rev.* B **31** 805
[42] Wenzien B, Käckell P and Bechstedt F 1994 *Proc. ICPS-22 (Vancouver 1994)* (Singapore: World Scientific) p 389
[43] Wenzien B, Käckell P and Bechstedt F 1995 *Surf. Sci.* **331–333** 1105
[44] Furthmüller J, Bechstedt F, Hüsken H, Schröter B and Richter W 1998 *Phys. Rev.* B **58** 13712
[45] Starke U, Schardt J, Bernhardt J, Franke M, Reuter K, Wedler H, Heinz K, Furthmüller J, Käckell P and Bechstedt F 1998 *Phys. Rev. Lett.* **80** 758
[46] Starke U 1997 *Phys. Status Solidi* b **202** 475
[47] Kaplan R 1989 *Surf. Sci.* **215** 111
[48] Nakanishi S, Tokutaka H, Nishimori K, Kishida S and Ishihara N 1989 *Appl. Surf. Sci.* **41/42** 44
[49] Bermudez V M and Kaplan R 1991 *Phys. Rev.* B **44** 11149
[50] Starke U, Bram Ch, Steiner P-R, Hartner W, Hammer L, Heinz K and Müller K 1995 *Appl. Surf. Sci.* **89** 175
[51] Schardt J, Bram Ch, Müller S, Starke U, Heinz K and Müller K 1995 *Surf. Sci.* **337** 232
[52] Owman F and Mårtensson P 1995 *Surf. Sci.* **330** L639
[53] Li L and Tsong I S T 1996 *Surf. Sci.* **351** 141
[54] Hollering M, Ziegler A, Graupner R, Mattern B, Ley L, Stampfl A P J, Riley J D, Leckey R C G, Bernhardt J, Schardt J, Starke U and Heinz K 1997 *Diamond Relat. Mater.* **6** 1997
[55] Johansson L I, Owman F and Mårtensson P 1996 *Surf. Sci. Lett.* **360** L478
[56] Themlin J M, Forbeaux I, Langlais V, Belkhir H and Debever J M 1997 *Europhys. Lett.* **39** 61
[57] Benesch C, Fartmann M and Merz H 2001 *Phys. Rev.* B **64** 205314
[58] Johansson L S O, Duda L, Laurenzis M, Krieftewirth M and Reihl B 2000 *Surf. Sci.* **445** 109
[59] Ahn J R, Lee S S, Kim N D, Hwang C G, Min J H and Chung J W 2002 *Surf. Sci. Lett.* **516** L529
[60] Northrup J E and Neugebauer J 1998 *Phys. Rev.* B **57** R4230
[61] Santoro G, Scandolo S and Tosatti E 1999 *Phys. Rev.* B **59** 1891
[62] Bechstedt F *et al* 2004 *J. Phys.: Condens. Matter* **16** S1721
[63] Coati A, Sauvage-Simkin M, Garreau Y, Pinchaux R, Argunova T and Aid K 1999 *Phys. Rev.* B **59** 12224
[64] Ramachandran V and Feenstra R M 1999 *Phys. Rev. Lett.* **82** 1000
[65] Johansson L S O, Duda L, Laurenzis M, Krieftewirth M and Reihl B 2000 *Surf. Sci.* **445** 109
[66] Kulakov M A, Henn G and Bullemer B 1996 *Surf. Sci.* **346** 49
[67] Dayan M 1986 *J. Vac. Sci. Technol.* A **4** 38
[68] Parill T M and Bermudez V M 1987 *Solid State Commun.* **63** 231
[69] Bermudez V M and Long J P 1989 *J. Appl. Phys.* **66** 6084
[70] Hara S, Slijkerman W F J, van der Veen J F, Ohdomari I, Misawa S, Sakuma E and Yoshida S 1990 *Surf. Sci. Lett.* **231** L196
[71] Powers J M, Wander A, Rous P J, Van Hove M A and Somorjai G A 1991 *Phys. Rev.* B **44** 11159
[72] Parill T M and Chung Y W 1991 *Surf. Sci.* **243** 96
[73] Yoshinobu T, Izumikawa I, Mitsui H, Fuyuki T and Matsunami H 1991 *Appl. Phys. Lett.* **59** 2844
[74] Fuyuki T, Yoshinobu T and Matsunami H 1993 *Thin Solid Films* **225** 225
[75] Hara S, Misawa S, Yoshida S and Aoyagi Y 1994 *Phys. Rev.* B **50** 4548
[76] Hara S, Kitamura J, Okushi H, Misawa S, Yoshida Y and Tokumaru Y 1996 *Surf. Sci.* **357/358** 436
[77] Shek M L 1996 *Surf. Sci.* **349** 317
[78] Semond F, Soukiassian P, Mayne A, Dujardin G, Douillard L and Jaussaud C 1996 *Phys. Rev. Lett.* **77** 2013
[79] Käckell P, Bechstedt F, Hüsken H, Schröter B and Richter W 1997 *Surf. Sci.* **391** L1183
[80] Soukiassian P, Semond F, Douillard L, Mayne A, Dujardin G, Pizzagalli L and Joachim C 1997 *Phys. Rev. Lett.* **78** 907
[81] Kitamura J, Hara S, Okushi H, Yoshida Y, Misawa S and Kajimura K 1999 *Surf. Sci.* **433–435** 465
[82] Duda L, Johansson L S O, Reihl B, Yeom H W, Hara S and Yoshida S 1999 *Surf. Sci.* **439** 199
[83] Douillard L, Fauxchoux O, Aristov V Y and Soukiassian P 2000 *Appl. Surf. Sci.* **166** 220
[84] Duda L, Johansson L S O, Reihl B, Yeom H W, Hara S and Yoshida S 2000 *Phys. Rev.* B **61** R2460

[85] Krüger P and Pollmann J 1995 *Phys. Rev. Lett.* **74** 1155
[86] Long J P, Bermudez V M and Ramaker D E 1996 *Phys. Rev. Lett.* **76** 991
[87] Yeom H W, Chao Y-C, Terada S, Hara S, Yoshida S and Uhrberg R I G 1997 *Phys. Rev.* B **56** R15525
[88] Yeom H W, Chao Y-C, Matsuda I, Hara S, Yoshida S and Uhrberg R I G 1998 *Phys. Rev.* B **58** 10540
[89] Yeom H W, Shimomura M, Kitamura J, Hara S, Tono K, Matsuda I, Mun B S, Huff W A R, Kono S, Ohta T, Yoshida S, Okushi H, Kajimura K and Fadley C S 1999 *Phys. Rev. Lett.* **83** 1640
[90] Shimomura M, Yeom H W, Mun B S, Fadley C S, Hara S, Yoshida S and Kono S 1999 *Surf. Sci.* **438** 237
[91] Derycke V, Soukiassian P, Mayne A and Dujardin G 2000 *Surf. Sci.* **446** L101
[92] Catellani A, Galli G and Rigolli P L 2000 *Phys. Rev.* B **62** R4794
[93] Wang F H, Krüger P and Pollmann J 2002 *Phys. Rev.* B **66** 195335
[94] Bermudez V 2003 *Surf. Sci.* at press
[95] Krüger P and Pollmann J 2003 *at press*
[96] Bermudez V M and Long J P 1995 *Appl. Phys. Lett.* **66** 475
[97] Ostendorf R, Benesch C, Hagedorn M, Merz H and Zacharias H 2002 *Phys. Rev.* B **66** 245401
[98] Douillard L, Aristov V Y, Semond F and Soukiassian P 1998 *Surf. Sci. Lett.* **401** L395
[99] Benesch C, Merz H and Zacharias H 2001 *Surf. Sci.* **492** 225
[100] Hüsken H, Schröter B and Richter W 1998 *Surf. Sci.* **407** 114
[101] Aristov V Y, Douillard L, Fauxchoux O and Soukiassian P 1997 *Phys. Rev. Lett.* **79** 3700
[102] Enriquez H, Derycke V, Arsitov V Y, Soukiassian P, Le Lay G, di Cioccio L, Cricenti A, Croti C, Ferrari L and Perfetti P 2000 *Appl. Surf. Sci.* **162/163** 559
[103] Widstrand S M, Johansson L S O, Magnusson K O, Larsson M I, Yeom H W, Hara S and Yoshida S 2001 *Surf. Sci.* **479** 247
[104] Powers J M, Wander A, Van Hove M A and Somorjai G A *Surf. Sci.* **260** L7
[105] Catellani A, Galli G, Gygi F and Pellacini F 1998 *Phys. Rev.* B **57** 12255
[106] Shek M L, Miyano K E, Dong Q Y, Callcott T A and Ederer D L 1994 *J. Vac. Sci. Technol.* A **12** 1079
[107] Käckell P, Furthmüller J and Bechstedt F 1996 *Appl. Surf. Sci.* **104/105** 45
Käckell P, Furthmüller J and Bechstedt F 1997 *Diamond Relat. Mater.* **6** 1346
[108] Lu W, Krüger P and Pollmann J 1998 *Phys. Rev. Lett.* **81** 2292
[109] Douillard L, Semond F, Aristov V Y, Soukiassian P, Delley B, Mayne A, Dujardin G and Wimmer E 1998 *Mater. Sci. Forum* **264–268** 379
[110] Aristov V Y, Enriquez H, Derycke V, Soukiassian P, Le Lay G, Grupp C and Taleb-Ibrahimi A 1999 *Phys. Rev.* B **60** 16553
[111] Derycke V, Fonteneau P and Soukiassian P 2000 *Phys. Rev.* B **62** 12660
[112] Shevlin S A and Fisher A J 2000 *Phys. Rev.* B **62** 6904
[113] Soukiassian P, Aristov V Y, Douillard L, Semond F, Mayne A, Dujardin G, Pizzagalli L, Joachim C, Delley W and Wimmer E 1999 *Phys. Rev. Lett.* **82** 3721
[114] Lu W, Krüger P and Pollmann J 1998 *Phys. Rev. Lett.* **82** 3722
[115] Soukiassian *et al* 2003 *J. Phys.: Condens. Matter* **15**
[116] Catellani A, Galli G and Gygi F 1998 *Appl. Phys. Lett.* **72** 1902
[117] Pehlke E and Scheffler M 1993 *Phys. Rev. Lett.* **71** 2338
[118] Pasquarello A, Hybertsen M S and Car R 1996 *Phys. Rev.* B **53** 10942
[119] Rohlfing M, Krüger P and Pollmann J 1997 *Phys. Rev.* B **56** 2191
[120] Pollmann J, Krüger P and Lu W 2000 *Mater. Sci. Forum* **338–342** 369
[121] Lu W, Krüger P and Pollmann J 1999 *Phys. Rev.* B **60** 2495
[122] Lindner K 1997 *Diploma Thesis* Technical University Chemnitz
[123] Lübbe M, Lindner K, Sloboshanin S, Tautz S, Schäfer J and Zahn D R T 1998 *J. Vac. Sci. Technol.* A **16** 3471
[124] Benesch C, Merz H and Zacharias H 2002 *Phys. Rev.* B **65** 235317
[125] Yeom H W, Matsuda I, Chao Y-C, Hara S, Yoshida S and Uhrberg R I G 2000 *Phys. Rev.* B **61** R2417
[126] Derycke V, Soukiassian P, Amy F, Chabal Y, D'Angelo M D, Enriquez H B and Silly M 2003 *Nature Mater.* **2** 253
[127] Shevlin S A, Fisher A J and Hernandez E 2001 *Phys. Rev.* B **63** 195306
[128] Pizzagalli L, Catellani A, Galli G, Gygi F and Baratoff A 1999 *Phys. Rev.* B **60** R5129
[129] Lu W, Schmidt W G, Briggs E L and Bernholc J 2000 *Phys. Rev. Lett.* **85** 4381
[130] Rossow U, Lindner K, Lübbe M, Aspnes D E and Zahn D R T 2000 *J. Vac. Sci. Technol.* B **16** 2355
[131] D'Angelo M, Enriquez H, Aristov V Y, Soukiassian P, Renaud G, Barbier A, Noblet M, Chiang S and Semond F 2003 *J. Vac. Sci. Technol.* B at press
[132] Lu W, Krüger P and Pollmann J 2000 *Phys. Rev.* B **61** 2680
[133] Soukiassian P, Semond F, Mayne A and Dujardin G 1997 *Phys. Rev. Lett.* **79** 2498